



UNIVERSITY OF NAPLES “FEDERICO II”

NEUROSCIENCE PhD

Brain intra- and extra-cellular Sodium Concentration

in Multiple Sclerosis: A 7 Tesla MRI study

TUTORS:
Prof. P.B. Carrieri
Prof. M. Inglese

PhD STUDENT:
Dr. M. Petracca

INDEX

PART 1	An overview on ^{23}Na MRI in Multiple Sclerosis	Pag. 4
	Introduction	Pag. 5
	Biology of ^{23}Na	Pag. 7
	Role of ^{23}Na in the pathogenesis of MS	Pag. 7
	^{23}Na imaging techniques	Pag. 13
	Results of ^{23}Na MRI application in clinical studies	Pag. 14
	Conclusions	Pag. 20
PART 2	Non-invasive quantification of intra- and extra- cellular brain ^{23}Na in Multiple Sclerosis using ultrahigh-field MRI.	Pag. 21
	Introduction	Pag. 22
	Materials and Methods	Pag. 25
	Results	Pag. 34
	Discussion	Pag. 45

PART 3 Brain intracellular ²³Na concentration: Pag. 52

A window on age-related microstructural changes

Introduction Pag. 53

Material and methods Pag. 56

Results Pag. 60

Discussion Pag. 67

Copyright acknowledgment Pag. 70

References Pag. 71

PART 1

An overview on ^{23}Na MRI in Multiple Sclerosis

Introduction

Multiple Sclerosis (MS) is the most common cause of non-traumatic disability in young adults and affects more than two million people worldwide. The disease etiology is unknown but MS prevalence increases with increasing distance north or south of the equator and the risk of developing MS correlates with the place of residence during childhood; it is therefore believed that an early exposure to an unidentified infectious agent could trigger the disease in individuals with a favorable genetic background (alleles of the MHC DR4, DR15 and DQ6) (Compston and Coles, 2008; International MS Genetics *et al.*, 2013). MS is characterized by an inflammatory component, which is responsible for acute occurrence of clinical relapses and development of focal lesions and by a degenerative component, which is responsible for accrual of progressive physical and cognitive disability (Compston and Coles, 2008). In about 80% of cases, the disease onset is characterized by a subacute and transient neurological deficit (clinically isolated syndrome), while, in the remaining 20%, the disease causes, from the beginning, a gradual clinical worsening over time (primary progressive MS). After the first episode, the presence of dissemination in time and space is required in order to confirm the diagnosis of MS (Polman *et al.*, 2011). MS clinical course is usually characterized, during the initial stage, by unpredictable clinical and radiological relapses (relapsing-remitting MS -RR-MS); over time the recurrence of relapses tends to decrease and a gradual neurological worsening occurs (secondary progressive MS).

The etiology of MS is still unknown but the pathogenetic process seems to start in the periphery with the priming of myelin-autoreactive T lymphocytes, which, crossing the blood brain barrier, mediate an acute autoimmune reaction against myelin and cause the activation of resident microglia and infiltrated macrophages. Auto-reactive CD4⁺ T cells secreting interferon-gamma and interleukin-17 are among the main mediators of the pathological process. The release of inflammatory mediators (nitric oxide,

reactive oxygen species, myeloperoxidase, tumor necrosis factor- α) causes oligodendrocytes damage and myelin sheets disruption, and contributes to neuro-axonal damage and loss (Waxman, 2008).

In addition to inflammation, axonal damage can be driven or amplified by a number of other pathological processes including Wallerian degeneration following axonal transection due to focal lesions (Trapp *et al.*, 1998), lack of trophic support from myelin (Nave and Trapp, 2008), mutation of mitochondrial DNA (Dutta *et al.*, 2006; Campbell *et al.*, 2011), astrocytes dysfunction (Cambron *et al.*, 2012), glutamate excitotoxicity (Pitt *et al.*, 2000), iron accumulation (Lassmann *et al.*, 2012; Lassmann, 2014) and sodium (^{23}Na) ions accumulation (Smith, 2007).

Studies in experimental models of MS and in *post-mortem* samples from MS patients have provided evidence for the presence of over-expression and increased activation of persistent ^{23}Na channels in demyelinated axons and MS plaques (Moll *et al.*, 1991; Craner *et al.*, 2004; O'Malley *et al.*, 2009).

Brain ^{23}Na MRI has been introduced almost twenty years ago but poor signal to noise ratio (SNR) led to relatively long imaging times and/or poor spatial resolution compared to proton (^1H) MRI and the sparse availability of MRI scanners with broadband capability limited its use. Recent technological advances in MRI hardware and software and the availability of ultra-high field magnets have prompt new developments that permit better spatial resolution with shorter imaging times and better quantitative measurements of tissue ^{23}Na concentration (Boada FE, 1997; Thulborn *et al.*, 1999b). Over time, various invasive methods have been used to measure ^{23}Na content in animals and *ex vivo* human brain tissue (Woodward *et al.*, 1967; Winter *et al.*, 1998; Winter and Bansal, 2001). Non-invasive determination of brain ^{23}Na concentration with ^{23}Na imaging has shown to be equivalent to invasive biochemical *ex vivo* techniques (Thulborn *et al.*, 1999a).

Currently, there are eleven FDA-approved disease-modifying treatments for MS with a partial efficacy in decreasing relapse rate and accumulation of white matter (WM) lesions. Since none of them is effective on the neurodegenerative component of the disease, there is an unmet need for a reliable, non-

invasive technique that could help understanding the mechanisms responsible for neurodegeneration and be used for monitoring the response to new, neuroprotective therapies when they become available. In this overview we summarize the main findings obtained by the application of ^{23}Na imaging in preclinical and clinical studies, their importance in the light of ^{23}Na role in MS pathogenesis and their implications for disease monitoring and therapeutics development.

Biology of ^{23}Na

^{23}Na yields the second strongest nuclear magnetic resonance (NMR) signal among biologically relevant NMR-active nuclei. In the brain, ^{23}Na has a bicompartimental distribution with higher concentration (140 mmol/L) in the extracellular space and a lower concentration (ranging from 10 to 15 mmol/L) in the intracellular space. ^{23}Na has a critical role in several cellular functions such as mitosis, cellular proliferation, generation and propagation of action potentials and cell volume regulation (Hodgkin and Huxley, 1952; Koch and Leffert, 1979; Lang, 2007). To ensure the maintenance of tissue homeostasis and the preservation of intracellular structures and processes, ^{23}Na concentration is strictly controlled by the ATP-driven Na/K pump; pathological changes that determine an expansion of the extracellular space (e.g. tissue injury, edema or necrosis) or functional impairment of the Na/K pump are therefore expected to result in an increased tissue ^{23}Na concentration (Cameron *et al.*, 1980; Nagy *et al.*, 1983; Jain, 1987; Thulborn *et al.*, 2005).

Role of ^{23}Na in the pathogenesis of MS

Nerve fibers conduction is generated and propagated by activation of ^{23}Na channels, which, in intact myelinated axons, are clustered in the Ranvier nodes, enabling fast saltatory conduction; in unmyelinated axons, the distribution of ^{23}Na channels is more homogeneous along the axonal

membrane and conduction is slower and continuous. ^{23}Na ions, entering the nerve through voltage gated ^{23}Na channels, have to be actively extruded via an energy dependent process; therefore the greater the ^{23}Na influx, the greater the energy demand the neuron needs to fulfill (Trapp and Stys, 2009).

When demyelination occurs, ^{23}Na channels are redistributed from the Ranvier nodes to long segments of demyelinated membrane. Demyelinated axons express two voltage-dependent ^{23}Na channel isoforms: Nav1.2, which is normally present along premyelinated axons, and Nav1.6, which is the predominant isoform at normal Ranvier nodes. Nav1.6 channels produce a persistent current that is able to drive reverse Na/Ca exchange even in the absence of action potentials (Rush *et al.*, 2005).

While channels re-distribution represents an adaptive mechanism to preserve action potential conduction and facilitate recovery of neurological deficits, it imposes a huge burden on the axonal metabolism thus increasing the risk of axonal damage secondary to energy deprivation (England *et al.*, 1991; Craner *et al.*, 2004). In MS, the state of virtual hypoxia secondary to mitochondrial dysfunction (Waxman, 2006b; Lassmann, 2007) determines a decrease in ATP production, which, associated to the increased energy request needed to guarantee conduction along demyelinated axons, causes neuronal energy failure (Dutta *et al.*, 2006). Since the maintenance of ^{23}Na balance is an active process controlled by the Na/K pump, the ATP deficit induces intracellular ^{23}Na accumulation and reverse activation of Na/Ca exchanger; the activation of the ^{20}Ca dependent proteases and the cytoskeleton disruption represent the final step leading to cellular death (**Fig. 1**) (Stys, 2005; Waxman, 2008; Frischer *et al.*, 2009; Trapp and Stys, 2009; Lassmann *et al.*, 2012). Increased concentrations of intracellular ^{23}Na stimulate further ^{20}Ca accumulation by release from the endoplasmic reticulum, triggered by inositol 1,4,5-trisphosphate receptors and ryanodine receptors (**Fig. 1**) (Nikolaeva *et al.*, 2005).

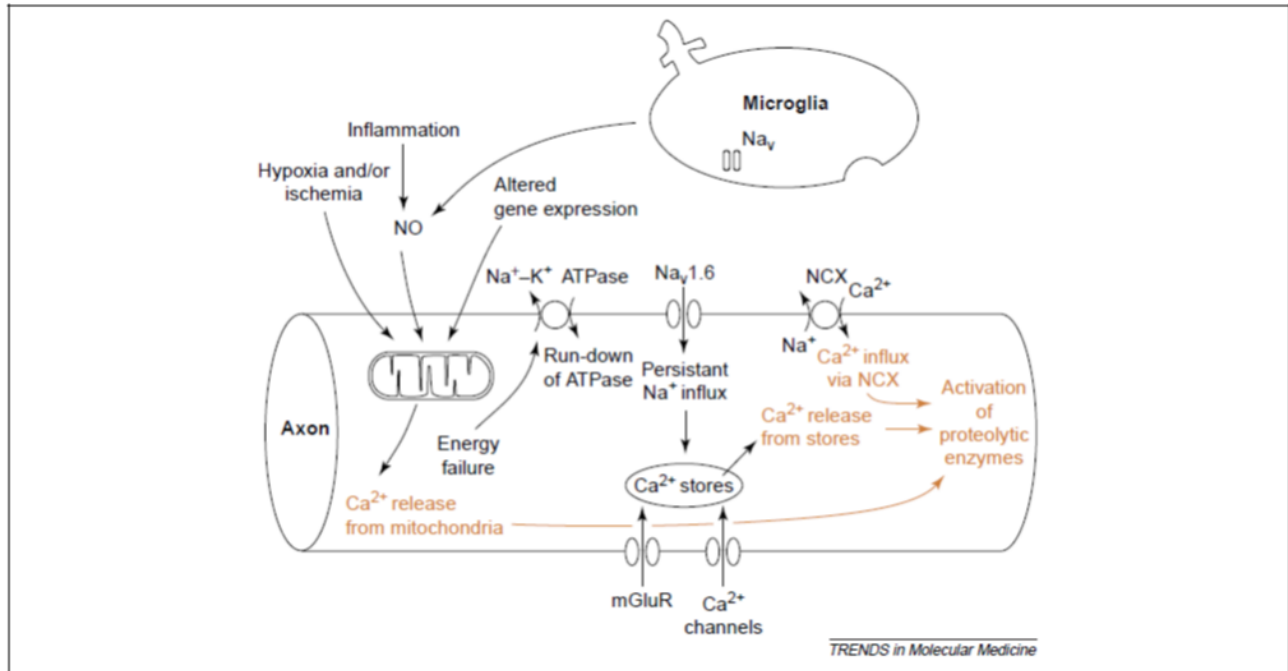


Fig. 1. Role of ^{23}Na channels in the axon degeneration cascade. Mitochondrial damage determines energy failure, with ATP deprivation and loss of function of Na/K ATPase. Consequent loss of ionic transmembrane gradient activates Nav1.6 channels producing a sustained ^{23}Na influx and reversing the operation of the Na/Ca exchanger. Further ^{20}Ca release into the axoplasm occurs from injured mitochondria and intracellular stores, triggered by inositol 1,4,5-trisphosphate receptors and ryanodine receptors, stimulate by increased intracellular ^{23}Na concentrations. Elevated intracellular levels of ^{20}Ca activate downstream proteolytic cascade, which produce axonal injury. Reproduced from Waxman 2006 (Elsevier Ltd.)

In summary, the two key factors leading to abnormal ^{23}Na influx in MS are (i) the defective mitochondrial function and (ii) the ^{23}Na influx via Nav1.6 channels (Waxman, 1977; Stys *et al.*, 1992b; Rush *et al.*, 2005); however, their relative contribution to axonal injury is still unclear.

Supporting this hypothesis, over expression of ^{23}Na channels along demyelinated axons (Moll *et al.*, 1991; Craner *et al.*, 2004) and upregulation of ^{23}Na channels in activated macrophages, microglia and astrocytes (Craner *et al.*, 2005; Black *et al.*, 2010) have been reported in MS plaques (**Fig. 2**).

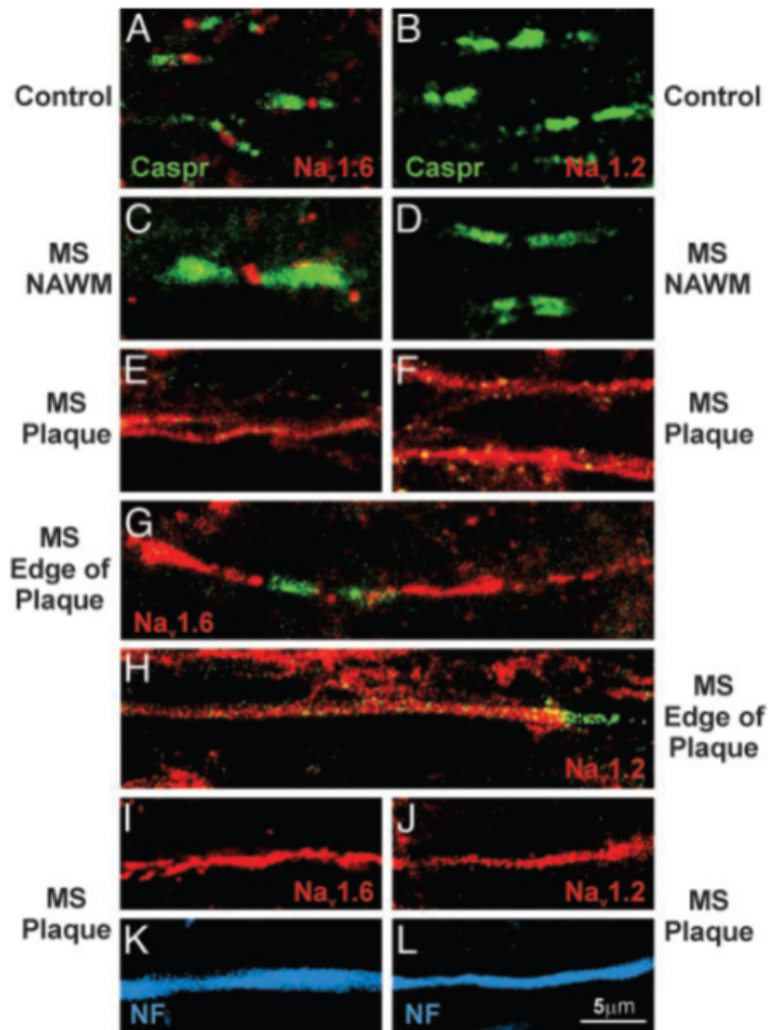


Fig. 2. Altered axonal expression of ^{23}Na channels in MS. Sections of postmortem spinal cord white matter from control (A and B) and MS (C–L) patients, immunostained to show Nav1.6 (red), Nav1.2 (red), Caspr (integral constituent of paranodal junctions-green), and neurofilaments (blue). In control white matter (A) and in normal-appearing white matter in MS tissue (C), Nav1.6 is localized at nodes of Ranvier whereas Nav1.2 is not detectable (B and D). Within MS plaques, continuous Nav1.6 (E) and Nav1.2 (F) immunostaining are present; in some instances bounded by Caspr (G-H). Colocalization of Nav1.6 (I) and Nav1.2 (J) with neurofilament immunostaining (K and L; blue) confirms the axonal identity of these profiles. Reproduced from Craner et al. 2004 Copyright (2004) National Academy of Sciences, U.S.A.

Moreover, it has been shown that in the animal models of experimental autoimmune encephalomyelitis (EAE), the mutation of the ^{23}Na channel subunit, which controls the expression of ^{23}Na channels on the cells surfaces, determines reduced axonal degeneration and neurological disability (O'Malley *et al.*, 2009). Adaptation to the increased energy demand has been reported not only in lesions and normal appearing white matter (NAWM) but also in the normal appearing grey matter (GM), where pathological studies have shown an increased mitochondrial density (Blokhin *et al.*, 2008). Moreover, the ^{23}Na related damage in the GM could be linked to the presence of cortical demyelinating lesions and to the abnormal neuronal expression of ^{23}Na channels with atypical properties, as exemplified by the expression of Nav1.8 channels, resistant to inactivation, in the Purkinje neurons of animals with EAE and patients with progressive MS (Black *et al.*, 2000).

Since ^{23}Na channels upregulation is responsible for axonal degeneration, ^{23}Na channels blockers are expected to exert neuroprotective effects. Indeed, state-dependent ^{23}Na channels blockers (e.g. class I anti-arrhythmic or anticonvulsants) are able to protect axons from anoxic-ischemic injury *in vitro* (Stys *et al.*, 1992a; Stys *et al.*, 1992b; Fern *et al.*, 1993; Stys, 1995; Stys and Lesiuk, 1996) and in animal models of MS (Lo *et al.*, 2003; Bechtold *et al.*, 2004; Bechtold *et al.*, 2006; Black *et al.*, 2007; Al-Izki *et al.*, 2014), at concentrations that do not compromise the conduction of action potentials. This is further supported by the demonstration that the abrupt withdrawal of phenytoin and carbamazepine seems to induce disease exacerbation and increase of the inflammatory markers in EAE (Black *et al.*, 2007).

These findings have prompt clinical trials to investigate the neuroprotective effect of voltage-gated ^{23}Na channel blockers in patients with MS. Unfortunately, the first clinical trial assessing the neuroprotective effect of lamotrigine in MS patients failed to show an effect on brain atrophy accrual. In particular, cerebral volume of patients treated with lamotrigine did not differ from that of placebo over 24 months; moreover, lamotrigine seemed to cause early volume loss that reversed partially on

discontinuation of treatment. In contrast with the pseudoatrophy described over the first few months of therapy with other immunomodulatory agents, the decrease in cerebral volume during lamotrigine treatment occurred slowly over 6-12 months and was not associated with reduction in relapse rate and MRI activity; it is therefore possible that it reflected the development of actual axonal loss (Kapoor *et al.*, 2010). Although the treatment failure may in part be explained by the high rate of non-adherence to therapy in the lamotrigine group, it is also possible that the decrease of cells volume induced by reduced entry of ^{23}Na ions and water caused by ^{23}Na channel blockade and the lamotrigine anti-inflammatory activity within normal-appearing tissue may have contributed to the results.

Even if the direct blockage of ^{23}Na voltage channel has not produced the expected results in the lamotrigine trial (Kapoor *et al.*, 2010), the systemic administration of amiloride, and the consequent blockage of ^{23}Na and ^{20}Ca influx through the proton-gated acid-sensing ion channel 1, has proven a neuroprotective effect not only in acute and chronic experimental models of MS (Friese *et al.*, 2007; Vergo *et al.*, 2011), but also in progressive MS patients (Arun *et al.*, 2013).

There are a few ongoing trials testing the efficacy of ^{23}Na channel blockers in different MS phenotypes (see ClinicalTrials.gov for details) and, therefore, once validated in longitudinal studies, ^{23}Na imaging might prove useful in providing an additional measure of cellular and metabolic brain changes during treatment with ^{23}Na blockers.

^{23}Na imaging techniques

Single quantum (SQ) ^{23}Na MRI is an imaging technique that exploits the magnetic resonance properties of ^{23}Na atomic nuclei, allowing the metabolic characterization of brain tissue *in vivo*. Unlike other metabolic imaging techniques (e.g. MR spectroscopy) it allows exploration and quantitative assessment of brain metabolism both at a global and regional level. Unfortunately, since the concentration of ^{23}Na

ions in the human body is much lower than ^1H concentration, ^{23}Na MRI presents a poor SNR, which is responsible for the longer acquisition time and the poor spatial resolution of ^{23}Na MRI in comparison to standard ^1H MRI. In addition, in most biologic tissues, ^{23}Na interactions with macromolecules determines a bi-exponential transverse relaxation time (T2) with the signal main component (up to 60%) hardly detectable due to its short echo time (Maudsley and Hilal, 1984).

These technical limitations have been partially overcome by the development of ultra-short TE sequences (Boada FE, 1997) and the availability of ultra-high field magnets (Thulborn *et al.*, 1999b) leading to a rekindled interest and application of brain ^{23}Na imaging in neurological diseases such as ischemic stroke, brain tumors and Alzheimer's disease (Thulborn *et al.*, 1999b; Ouwerkerk *et al.*, 2003; Mellon *et al.*, 2009).

^{23}Na MRI quantifies the tissue total sodium concentration (TSC), which represents the weighted average of intracellular and extracellular ^{23}Na (respectively 10-15 mmol/L and 140 mmol/L). TSC is sensitive to changes in both extra- and intra-cellular space, being affected by cellular death, swelling, proliferation (Jain, 1987; Thulborn *et al.*, 2005) as well as by metabolic changes that affect ^{23}Na exchange across the cell membrane (Cameron *et al.*, 1980; Nagy *et al.*, 1983). In the CNS, we may therefore assume that TSC increase is related to intra-axonal accumulation of ^{23}Na ions, determined by Na/K pump dysfunction, as well as to enlargement of extra-axonal space consequent to neuronal degeneration.

Results of ^{23}Na MRI application in clinical studies

The first application of ^{23}Na MRI in patients with MS has been reported by Inglese *et al.* (Inglese *et al.*, 2010b) and has demonstrated that patients with RR-MS show higher NAWM TSC in comparison with healthy controls; such increase in ^{23}Na concentration is even higher in acute and chronic lesions compared to areas of NAWM. In addition, TSC levels in lesions, NAWM and GM showed a direct

correlation with T2-weighted and T1-weighted lesion load while NAGM TSC was found to be negatively associated with GM volume. In the same study the EDSS (Expanded Disability Status Scale) (Kurtzke, 1983) showed a mild, positive association with the mean TSC value in chronic lesions, NAWM and GM. These results suggest that the abnormal increase of TSC in MS patients might reflect changes in cellular and metabolic integrity of WM lesions as well as normal appearing brain tissue. These findings have been reproduced in different laboratories around the world and the application of the method has been extended to patients with clinical phenotypes other than RR-MS (Zaaraoui *et al.*, 2012; Paling *et al.*, 2013; Maarouf *et al.*, 2014). In MS patients at early disease stage ^{23}Na increase seems to be limited to macroscopic lesions (Zaaraoui *et al.*, 2012) while in patients with longer disease duration (>5 years) TSC appears to be increased not only in lesions, but also in NAWM, cortical and deep GM (Inglese *et al.*, 2010b; Zaaraoui *et al.*, 2012; Paling *et al.*, 2013) with higher concentration reported in more destructive lesions (**Fig. 3**) (Inglese *et al.*, 2010b; Paling *et al.*, 2013) and in patients with progressive phenotypes (**Fig. 4**) (Paling *et al.*, 2013; Maarouf *et al.*, 2014).

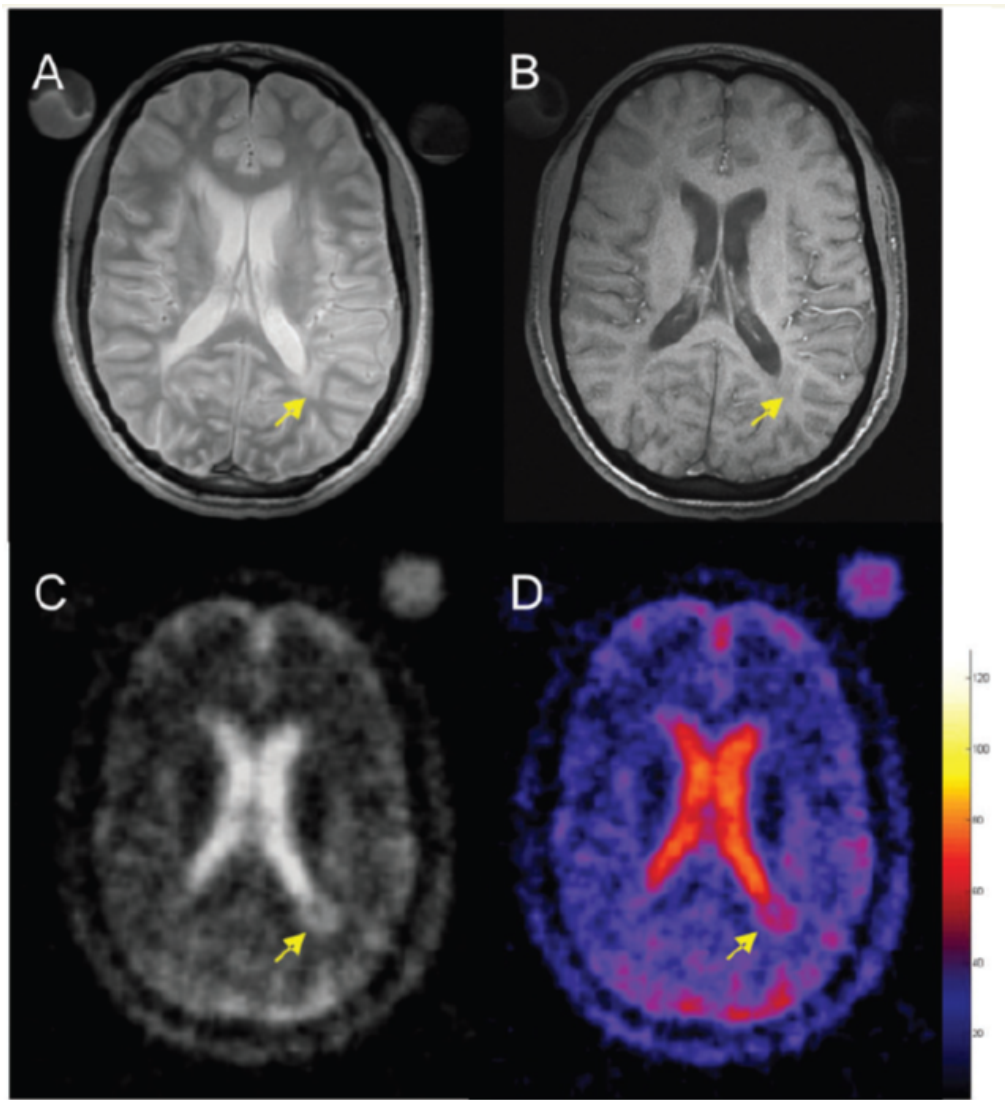


Fig. 3. Selected brain axial proton density (A), T1-weighted (B), ²³Na images (C) and corresponding TSC map (D) from an MS patient. The arrow indicates a hypointense periventricular lesion (B) that shows a higher TSC value. The color bar represents the TSC values (mM). Reproduced from Inglese et al. 2010 (Oxford University Press).

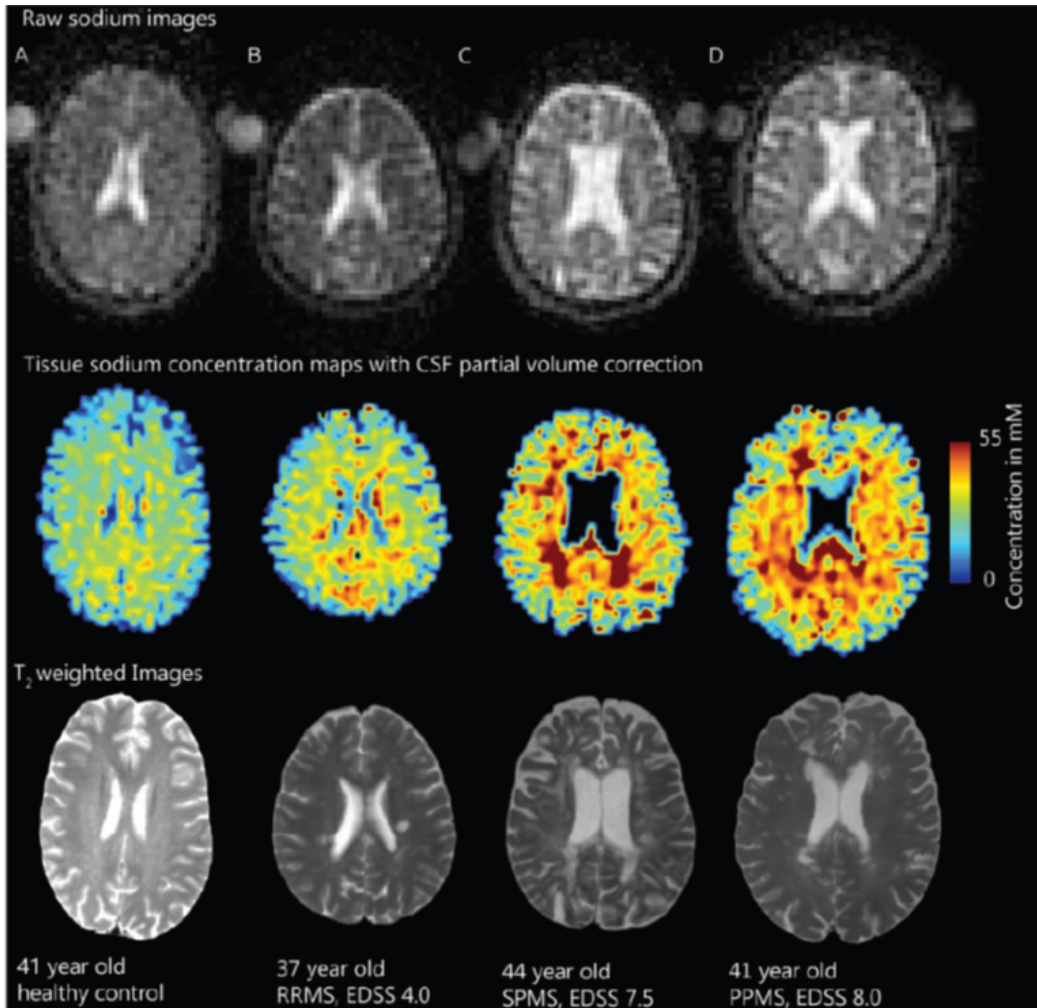


Fig. 4. Global ^{23}Na concentration across MS phenotypes. Raw ^{23}Na images in ^{23}Na space (top), tissue ^{23}Na maps with CSF partial volume correction (middle) and T2-weighted images (bottom) registered to the T1 volumetric scan in controls (A) and patients with MS (B-C-D). Increased ^{23}Na is seen in relapsing remitting- MS patients lesions (B) and, more extensively, in lesions and normal appearing white matter of secondary- (C) and primary- (D) progressive MS patients. Reproduced from Paling et al.2013 (Oxford University Press).

While TSC increase in lesions might be explained by gliosis, tissue disruption and replacement with extracellular fluid, TSC increase in normal appearing brain tissue might be related not only to increased extracellular space, caused by demyelination and axonal loss, but also to intra-axonal ^{23}Na increase.

Brain regional analysis of TSC distribution has shown a limited involvement of the NAWM (brainstem, cerebellum and temporal poles) in the early stage of the disease, and a widespread TSC increase, involving the entire brain, in more advanced MS (Zaaraoui *et al.*, 2012). In particular, while in PP patients TSC increase seems to be restricted to the motor system, in SP patients it is more diffuse, involving also frontal, limbic and visual cortex, deep GM and cerebellum (**Fig. 5**) (Maarouf *et al.*, 2014).

In both relapsing and progressive patients, TSC shows only a modest correlation with clinical disability (Inglese *et al.*, 2010b; Paling *et al.*, 2013) and a weak correlation with lesion load and GM atrophy (Inglese *et al.*, 2010b; Zaaraoui *et al.*, 2012). The correlation between TSC increase, clinical disability and MRI parameters of tissue loss, although present and consistently replicate across studies, is only modest; this could indicate that TSC reflects not only the irreversible neuronal loss responsible for clinical disability, but also the potentially reversible neuronal functional damage and could therefore be especially useful as predictive factor of clinical outcome. Supporting this hypothesis, only a small overlap has been identified between local brain atrophy and regions showing TSC increase (Maarouf *et al.*, 2014); moreover, disability seems to correlate with NAWM TSC but not with WM fraction (Paling *et al.*, 2013).

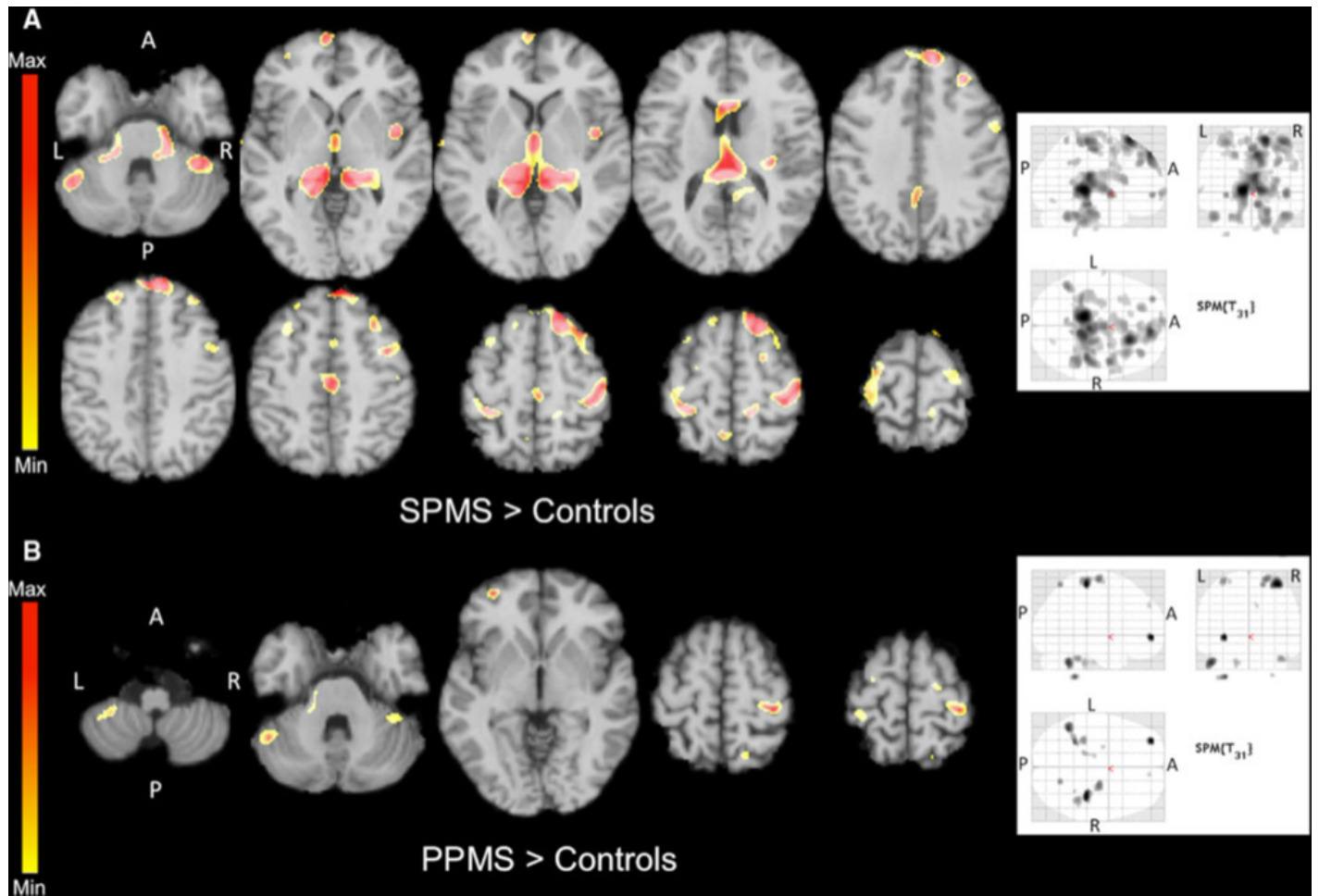


Fig. 5. Statistical mapping of TSC increases in secondary progressive MS patients relative to controls (A) and in primary progressive MS patients relative to controls (B). In order to reduce CSF contamination grey matter, normal appearing white matter and T2 lesion masks were applied onto the co-registered quantitative sodium concentration maps to obtain TSC distribution maps of each compartment for each patient. Reproduced from Maarouf et al. 2013 (Springer Ltd.)

Conclusions

^{23}Na MRI allows direct visualization, *in vivo*, of ongoing cellular metabolic dysfunction and death. Unfortunately, so far, the impossibility to determine if TSC increase is linked to an accumulation of intracellular ^{23}Na or an increase in extracellular volume represents a major limitation.

In Part 2 we present the first application, in MS patients, of a method combining single quantum (SQ) and triple quantum filtered (TQF) ^{23}Na MRI, to quantify TSC and the intracellular sodium molar fraction (ISMF) and then derive ISC and the ISVF, an indirect measure of ESC (the lower the ISVF, the higher the ESC).

In MS patients, TSC and ISC increase might indicate axonal dysfunction, offering insights in axonal metabolism before the generation of stable, irreversible, axonal damage they could be a putative target for therapeutic interventions (Nikic *et al.*, 2011) TSC and the more technically challenging ISC, might enable *in vivo* assessment of the metabolic state on the brain and identification of an ‘intervention window’, providing a better tool to investigate the neuroprotective effects of experimental therapies and to monitor the response to putative neuroprotective agents and ^{23}Na blockers in clinical trials. ^{23}Na imaging could also be helpful in studying and understanding the role of energy failure, clarifying MS pathophysiology in comparison with others neuroinflammatory conditions (e.g. neuromyelitis optica, and acute disseminated encephalomyelitis).

PART 2

Non-invasive quantification of intra- and extra- cellular brain ^{23}Na in Multiple Sclerosis using ultrahigh-field MRI.

Introduction

MS is the most common cause of non-traumatic neurological disability in young adults and has a high socio-economic impact, which increases as disability progresses (Noseworthy *et al.*, 2000). Although there is increasing evidence that neuro-axonal degeneration is a relevant cause of permanent disability (De Stefano *et al.*, 1998; Miller *et al.*, 2002; Bjartmar and Trapp, 2003; Frischer *et al.*, 2009; Tallantyre *et al.*, 2010; Filippi *et al.*, 2013), the pathophysiological mechanisms underlying neuroaxonal injury or loss are poorly understood and there are no therapeutic agents with proven efficacy in preventing or slowing the progressive accumulation of disability. Several histological and experimental studies have suggested that the increase of sodium influx in demyelinated axons could be one of the key mechanisms of delayed axonal injury and that partial blockade of sodium channels protects axons from degeneration in experimental models of MS (Lo *et al.*, 2003; Bechtold *et al.*, 2006; Black *et al.*, 2006; Black *et al.*, 2007; Waxman, 2008; Al-Izki *et al.*, 2014). Recent in vivo MRI studies using sodium (^{23}Na) imaging, have shown increased brain total sodium concentration (TSC) in patients with MS (Inglese *et al.*, 2010b; Zaaraoui *et al.*, 2012; Paling *et al.*, 2013; Maarouf *et al.*, 2014). Brain sodium concentration is increased both in lesions and normal-appearing brain tissue, especially in the advanced and progressive stages of the disease, and in patients with greater disability. TSC is a weighted average of intracellular sodium concentration (ISC ~ 10-15 mM) and extracellular sodium concentration (ESC~140 mM) and its increase in MS can result from neuro-axonal metabolic dysfunction (Trapp and Stys, 2009), and/or from the expansion of the extracellular space secondary to neuro-axonal loss or presence of edema (Perier and Gregoire, 1965; Turski *et al.*, 1986). However, TSC measurement does not allow discrimination between the two compartments and, therefore, the disease-related change in ISC and ESC and their relationship with structural MRI measures and clinical parameters is yet unknown.

The measurement of the MRI signal from ISC is quite challenging and can be performed *in vivo* with a few techniques that include the use of shift reagents, inversion recovery pulses, and multiple quantum filters (MQFs). MQFs is based on the different relaxation properties of the sodium nuclei in the extracellular and intra-cellular space, which generate a mono- and bi-exponential NMR signal decay, allowing the differentiation of the signal from the two compartments (Muller N *et al.*, 1987; Borthakur *et al.*, 1999; Hancu *et al.*, 1999). Despite its importance, *in vivo* measurement of ISC in humans has been hampered by technical challenges and the few examples of the application of MQFs ^{23}Na MRI to the human brain available in the literature are limited to case reports and qualitative results (Hancu *et al.*, 1999; Boada *et al.*, 2004).

Our group has recently implemented a MR pulse sequence for the acquisition of triple-quantum filtered (TQF) ^{23}Na MRI (Fleysher *et al.*, 2010b) and developed a non-invasive method which employs single quantum (SQ) and TQF imaging at 7 Tesla to quantify ISC and intracellular sodium volume fraction (ISVF), an indirect measure of ESC. Since the brain–sodium model considers the cell membrane a part of intracellular space, the term ISVF is a synonymous of cell volume fraction (cell volume divided by tissue volume). Therefore, an ISVF reduction indicates loss of the intracellular volume and reflects an increase of the extracellular space and, as a consequence, of ESC (Fleysher *et al.*, 2013a). We obtained quantitative mapping of ISC and ISVF maps in healthy volunteers, with ISC and ISVF values in good agreement with those obtained with invasive methods and/or *ex vivo* studies (Fleysher *et al.*, 2013a). Ultra-high field MRI is particularly suited for the application of this method, due to the relatively low sensitivity of ^{23}Na MRI.

The present study is the first to investigate the feasibility of ISC and ISVF measures in patients with MS. We sought to explore the hypothesis that while a decrease in ISVF would be associated with tissue loss as measured by conventional MRI techniques, an increase in ISC would not be associated reflecting axonal metabolic dysfunction rather than tissue destruction. Therefore, the aims of our study

were: i) to determine the feasibility of TQF ^{23}Na MRI in patients with MS at 7 Tesla; ii) to measure the global and regional brain distribution of TSC, ISC and ISVF; iii) to investigate the relationship between intra- and extra-cellular sodium concentration and measures of lesion and brain volume; iv) to evaluate the clinical impact of abnormal brain sodium distribution.

Materials and Methods

Subjects

Nineteen patients diagnosed with MS according to the McDonald criteria (McDonald *et al.*, 2001) and presenting a relapsing-remitting (Lublin and Reingold, 1996) course were prospectively enrolled in the present study. The exclusion criteria were: i) a current or past medical or psychiatric disorder other than MS; ii) current or past substance abuse, and/or iii) MS relapse or corticosteroid use in the previous 6 weeks. Disability was assessed by a single, experienced neurologist who was blind to the MRI findings, using the Expanded Disability Status Scale (EDSS) score (Kurtzke, 1983) within 1 week of MRI. All the patients were under immunomodulatory treatment with either interferon beta-1a or glatiramer acetate. Seventeen age- and gender-matched healthy volunteers were enrolled as control group. Demographic characteristics of the study populations are presented in Table 1. Approval for this study was obtained from the local Institutional Board of Research Associates, and informed consent was obtained from all subjects before study initiation.

MRI acquisition

All subjects underwent ^1H -MRI at 3T (Siemens Medical Solutions, Germany) and SQ and TQF ^{23}Na MRI at 7T (MAGNETOM, Siemens Healthcare) in two separate sessions on the same day of their clinical assessment. The 3T ^1H -MRI protocol included the following sequences: i) dual-echo turbo spin echo (repetition time [TR]=5000 ms; echo time [TE]=11 ms; 48 contiguous 3-mm thick axial slices) ii) 3D T_1 -weighted – magnetization-prepared rapid-acquisition gradient echo (TR=2400 ms; TE=2.71 ms; inversion time [TI]=900 ms; flip angle=12°; voxel size=1 mm³) iii) post-gadolinium (Gd) T_1 -weighted spin-echo (TR=354 ms; TE=2.73 ms; 50, 3 mm-thick axial slices). The sodium SQ and TQF protocol at 7T was acquired with a custom-built dual-tuned TX/RX $^1\text{H}/^{23}\text{Na}$ head coil (Wiggins *et al.*, 2010). SQ ^{23}Na MRI was acquired using a 3D gradient echo sequence (TR=150 ms, TE=6.8 ms, flip angle=90°,

field of view=240x240 mm², matrix=48x48, voxel size=5x5x5 mm³); TQF ²³Na MRI was acquired using a modified 3D gradient-echo sequence with a new 12-step phase-cycling B₀-corrected triple-quantum-filtered scheme (TR=150 ms, TE=6.8 ms, flip angle=90°, field of view=240x240x240 mm³, matrix 30x30x24, voxel size 8x8x10 mm³, τ₁=6.8 ms τ₂=150 ms, 2 averages) (Fleysher *et al.*, 2013a). For the purposes of TSC quantification, calibration phantoms with known sodium concentrations (50 and 100 mM/L) were placed into the field of view. For TQF B₀-correction, B₀-maps were computed from the phase difference between two SQ images acquired over 3.6min (TR=150ms) with TE=6.8ms and TE=8.8ms, respectively. The SQ image with TE=6.8ms was used for TSC calculation. B₁-maps were computed from the ratio of two additional SQ images acquired over 3.6 min with FA=60° and 120°, TR=150 ms using the double flip-angle method. Using the B₁-maps, B₁-correction was applied to SQ and TQF images (Fleysher *et al.*, 2013).

Image analysis

Image processing was performed off-line on a PC workstation. All images were assessed by consensus by two experienced observers who were blind to the patients' identity and clinical status.

Lesion volume assessment

T₂-hyperintense and T₁-hypointense white matter lesions were identified and outlined, for each patient, respectively on the dual echo and T₁-weighted images, using a semi-automated technique based on user-supervised local thresholding (Jim version 6; Xinapse Systems, Northants, England, <http://www.xinapse.com>).

Lesion Probability Maps (LPMs) assessment

For the patients group, LPMs were obtained using imaging analysis tools of the FMRIB Software Library FSL 5 (www.fmrib.ox.ac.uk/fsl/) as described in Rossi *et al.* (Rossi *et al.*, 2012). Briefly, the

procedure consisted of three steps: brain extraction, registration to standard-space and computation of the maps. First, the brain was extracted from the 3D T₁-weighted and T₂-weighted images using the brain extraction tool and then corrected for intensity non-uniformity (Smith, 2002). Next, a two-stage registration was performed to align the T₂ lesion masks of each patient to the Montreal Neurological Imaging 152 standard brain: (i) each lesion mask was linearly co-registered to the corresponding 3D T₁-weighted brain images with FMRIB's Linear Image Registration Tool using the transformation parameters derived by linearly registering the T₂-weighted on the 3D T₁-weighted image; (ii) each lesion mask previously registered on the 3D T₁-weighted brain image was nonlinearly registered on the standard brain template using the transformation parameters derived by nonlinearly registering the 3D T₁-weighted image on the standard brain template. Finally, the LPMs were generated by first merging and then averaging all the standard-space lesion masks. For each map, voxel intensity represents the frequency of lesion occurrence in that voxel. A threshold of 50% was used to include the peaks of the lesion frequency on the LPMs.

Brain volume assessment

Normalized brain volume, gray matter and white matter volumes were computed for all subjects on the 3D T₁-weighted sequence using FSL's SIENAX program (SIENAX; FMRIB Centre, Oxford, England) as described elsewhere (Battaglini *et al.*, 2012). To avoid tissue misclassification, T₂-weighted lesions were refilled with intensities matching the surrounding normal-appearing white matter (Battaglini *et al.*, 2012).

Sodium imaging post-processing

The computation of Na maps is based on the canonical brain–sodium tissue model (Thulborn *et al.*, 1999b; Ouwerkerk *et al.*, 2003), which assumes that sodium is distributed between only two compartments: intracellular and extracellular.

The canonical brain–sodium tissue model is described by a homogeneous intracellular compartment occupying volume V_{in} and a homogeneous extracellular compartment with volume V_{ex} . Next, M_{in} and M_{ex} are used to denote respective sodium contents in intra– and extracellular compartments. Using these notations, bulk tissue sodium concentration (ρ_T) and ISC (ρ_{in}) can be expressed as:

$$\rho_T = \frac{M_{in} + M_{ex}}{V_{in} + V_{ex}} \quad \rho_{in} = \frac{M_{in}}{V_{in}} \quad [1]$$

Furthermore, the ISVF (η_{in}) and intracellular sodium molar fraction (ISVF, χ) are defined as:

$$\eta_{in} = \frac{V_{in}}{V_{in} + V_{ex}} = \frac{\rho_{ex} - \rho_T}{\rho_{ex} - \rho_{in}} \quad \chi = \frac{M_{in}}{M_{in} + M_{ex}} = \frac{\rho_{in}}{\rho_T} \eta_{in} \quad [2]$$

where ρ_{ex} stands for ESC.

Combining equations [1] and [2], we obtain the ISC ρ_{in} and the ISVF η_{in} in terms of tissue sodium concentration ρ_T and intracellular sodium molar fraction χ :

$$\begin{cases} \rho_{in} = \frac{\chi \rho_T \rho_{ex}}{\rho_{ex} - (1 - \chi) \rho_T} \\ \eta_{in} = 1 - (1 - \chi) \frac{\rho_T}{\rho_{ex}} \end{cases} \quad [3]$$

This representation of ISC and ISVF in terms of TSC and ISMF is convenient because TSC and ISMF are MRI–assessable quantities. Therefore, once TSC and ISMF are measured, ISC and ISVF can be computed using equation [3]. Since ESC is maintained in a narrow range between 136 and 142 mmol/L and did not vary much among subjects throughout this work, we used $\rho_{ex}=140$ mmol/L.

As previously described (Fleysher *et al.*, 2013a), ISC and ISVF were quantified as follows: first, SQ and TQF images were acquired and corrected for B0 and B1 inhomogeneities as described in Fleysher *et al.* (Fleysher *et al.*, 2010b). Second, TSC maps were quantified in Image J1.36b on a voxel-by-voxel basis from the SQ images using a linear method, dependent on the calibration phantom, as described by Inglese *et al.* (Inglese *et al.*, 2010b). Third, single-quantum and triple-quantum images were combined with TSC maps using an in-house procedure developed in Matlab (Fleysher *et al.*, 2013a) and ISC and ISVF maps were computed.

The resulting concentration maps (**Fig. 1**) were further analyzed with a global approach to measure TSC, ISC and ISVF over the entire gray and white matter tissue and with a voxel-based approach to measure TSC, ISC and ISVF at a regional level.

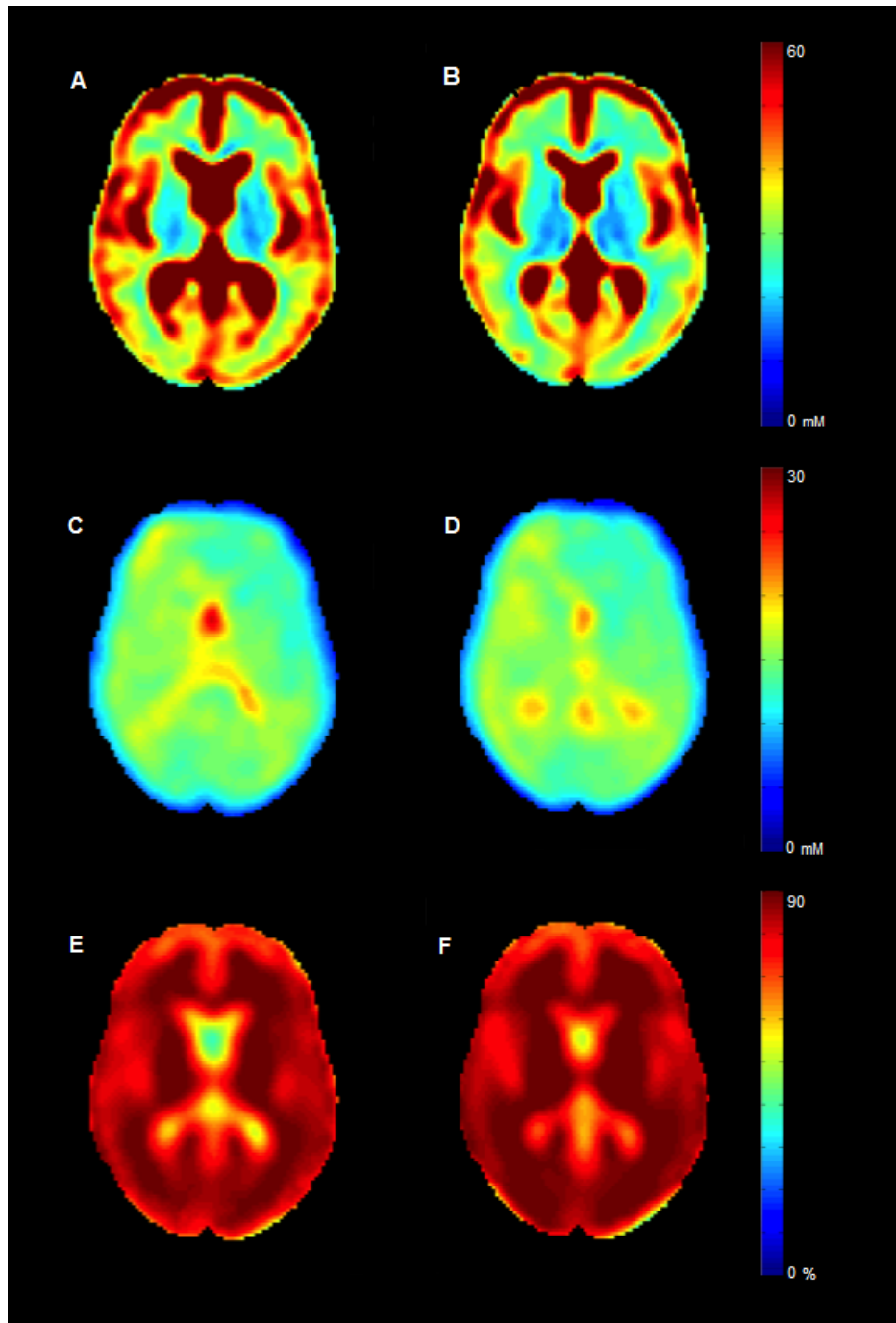


Fig. 1. ^{23}Na group maps. Mean TSC, ISC and ISVF maps for patients with MS (respectively A, C, E) and controls (respectively B, D, F). In both groups, TSC appears higher while ISC and ISVF are lower in grey matter than in white matter. Note that, since intracellular molar content and cell volume are equal to zero in extracellular tissue, ISVF and ISC measurements in CSF have to be considered meaningless.

Test-retest variance evaluation, conducted on three patients and three controls imaged on two separate occasions, at baseline and after 1 month (range 25 to 37 days), showed a coefficient of variation smaller than 5% for ISVF measures, ranging from 6% to 5% for TSC measures and from 10% to 6% for ISC measures.

Global analysis of sodium concentration

The analysis of the ^{23}Na concentration maps (i.e. TSC, ISC and ISVF maps) was performed with FSL 5 (<http://fsl.fmrib.ox.ac.uk/fsl/fslwiki>). The TSC maps were co-registered to the corresponding T_1 -weighted images with an affine-linear registration and the transformation matrices were saved. T_1 -weighted images were segmented and the obtained grey and white matter masks were superimposed onto ^{23}Na concentration maps in native ^{23}Na -image space using the inverse transformation matrix obtained in the step above; mean values from each tissue were extracted for each subject, obtaining grey matter, white matter and cerebrospinal fluid TSC, ISC and ISVF values. A probability of 50% was considered as threshold for grey and white matter tissue type classification due to the bigger voxel sizes and hence higher mixture of tissue type.

Sodium concentrations in T_2 - and T_1 -weighted lesions

Because of the limited spatial resolution of ISVF and ISC scans, only TSC was measured in T_2 - and T_1 -visible lesions. The assessment of sodium concentrations was performed with FSL 5 (<http://fsl.fmrib.ox.ac.uk/fsl/fslwiki>). First, the TSC maps were co-registered to the T_2 -weighted and 3D T_1 -weighted images with an affine linear registration using correlation ratio and trilinear interpolation. The generated inverse transformation matrix was applied to the lesions masks (including only lesions with a diameter equal or higher than 5 mm) in order to transfer them from the structural images space into the sodium native space. The T_2 - and T_1 -weighted lesions masks in sodium space were therefore superimposed on ^{23}Na concentration maps, obtaining mean TSC values in white matter lesions.

Voxel-based analysis of sodium concentration

The voxel-based processing on ^{23}Na concentration maps (i.e. TSC, ISC and ISVF maps) was performed with SPM8 (Wellcome Institute, London, England). For each patient, the ^{23}Na concentration maps were co-registered to the 3D T_1 -weighted image using normalized mutual information and trilinear interpolation. The 3D T_1 -weighted scans were spatially normalized into the Montreal Neurologic Institute space (VBM8); the transformation matrix between the native image space and the normalized stereotaxic Montreal Neurological Institute space with affine transformation and nonlinear warping generated during this process was applied to the co-registered ^{23}Na image maps, to reduce inter-individual differences. The partial volume effect was minimized by subtracting the cerebrospinal fluid segmented maps from each of the ^{23}Na concentration maps. Finally, the obtained quantitative ^{23}Na maps were smoothed with an 8-mm full width at half maximum Gaussian kernel for statistical mapping analysis. The Talairach Daemon Atlas from Wake Forest University Pickatlas toolbox from SPM8 (http://www.nitrc.org/projects/wfu_pickatlas) was used for grey matter labeling, whereas the JHU white matter tractography atlas from FSL was used (<http://www.fmrib.ox.ac.uk/fsl/data/atlas-descriptions.html#wm>) was used for white matter labeling.

Statistical analysis

SPSS version 20.0 (IBM, Chicago IL) was used for all statistical computations in terms of structural and global sodium parameters. Between-group comparisons of structural MRI parameters (brain volumes and lesion volumes) were assessed with an ANCOVA test, controlling for age and gender ($p < 0.05$). Between-group comparisons of global ^{23}Na concentrations (grey matter and white matter TSC, ISC and ISVF) were assessed with an ANCOVA test, controlling for age, gender and intra-cranial volume ($p < 0.05$). Within-group comparisons of global ^{23}Na concentrations (grey matter and white matter TSC, ISC and ISVF) were assessed with a paired sample t-test ($p < 0.05$).

Pearson bivariate correlation was applied to evaluate the association between sodium concentrations, age and disease duration.

A voxel-based statistical mapping analysis (SPM8) was used to assess regional brain differences in sodium concentration on the TSC compartments, using the spatially normalized TSC maps, and a two-groups ANCOVA test controlling for age, gender and intra-cranial volume ($p < 0.001$, corrected for family-wise error at $p < 0.05$, cluster extent 20 voxels). Then, the significant TSC clusters were extracted with MarsBaR toolbox (<http://marsbar.sourceforge.net/>) and used to restrict the ISC and ISVF voxel-based statistical mapping analysis, that was performed with a two-groups ANOVA ($p < 0.05$, cluster extent 10 voxels, uncorrected for multiple comparisons).

Partial correlations were assessed between global and regional ^{23}Na concentration, lesion and brain volumes, and clinical data (disease duration, EDSS score) controlling for age and gender ($p < 0.05$).

Due to the exploratory nature of this study, multiple testing correction was not performed and therefore the reported P values should be interpreted as descriptive. However, all analyses were performed with established a priori hypotheses. Correction for family wise error was only applied to the whole brain voxel wise comparison of TSC maps to avoid a massive multiple comparison penalty.

Results

Structural imaging

T₂-weighted, T₁-weighted lesion volumes and brain volumes are shown in **Table 1**. The anatomical distribution of T₂ lesions across the brain is shown in **Fig. 2**, super-imposed on the statistical parametric maps of brain sodium concentrations in MS patients. The peak of lesion frequency was localized in the right anterior thalamic radiation (39%). None of the patients presented Gd-enhancing lesions. Normalized brain volume, grey matter volume and white matter volume were decreased in MS patients compared to healthy controls (respectively $p < 0.01$, $p < 0.05$ and $p = 0.05$).

Table 1. Demographics characteristics and structural ¹H-MRI parameters in patients with MS and in healthy controls.

	MS patients	Healthy controls
Gender F:M	11:8	8:9
Age (years)	40.06 ±11.27	46.16 ±11.65
Disease duration (years)	9.11 ± 7.48	-
Median EDSS (range)	2.0 (0.0-5.5)	-
T ₂ lesion volume (mL)	6.61 ± 8.93	-
T ₁ lesion volume (mL)	1.79 ± 4.84	-
NBV (mL)	1415 ± 153.84**	1523.24 ± 57.96
GMV (mL)	744.47 ± 91.13*	793.76 ± 55.65
WMV (mL)	686.68 ± 76.46	735.59 ± 35.96

EDSS= Expanded Disability Status Scale; NBV= normalized brain volume; GMV= grey matter volume; WMV=white matter volume.

Unless otherwise specified data shown are mean ± standard deviation; *p<0.05; **p<0.01

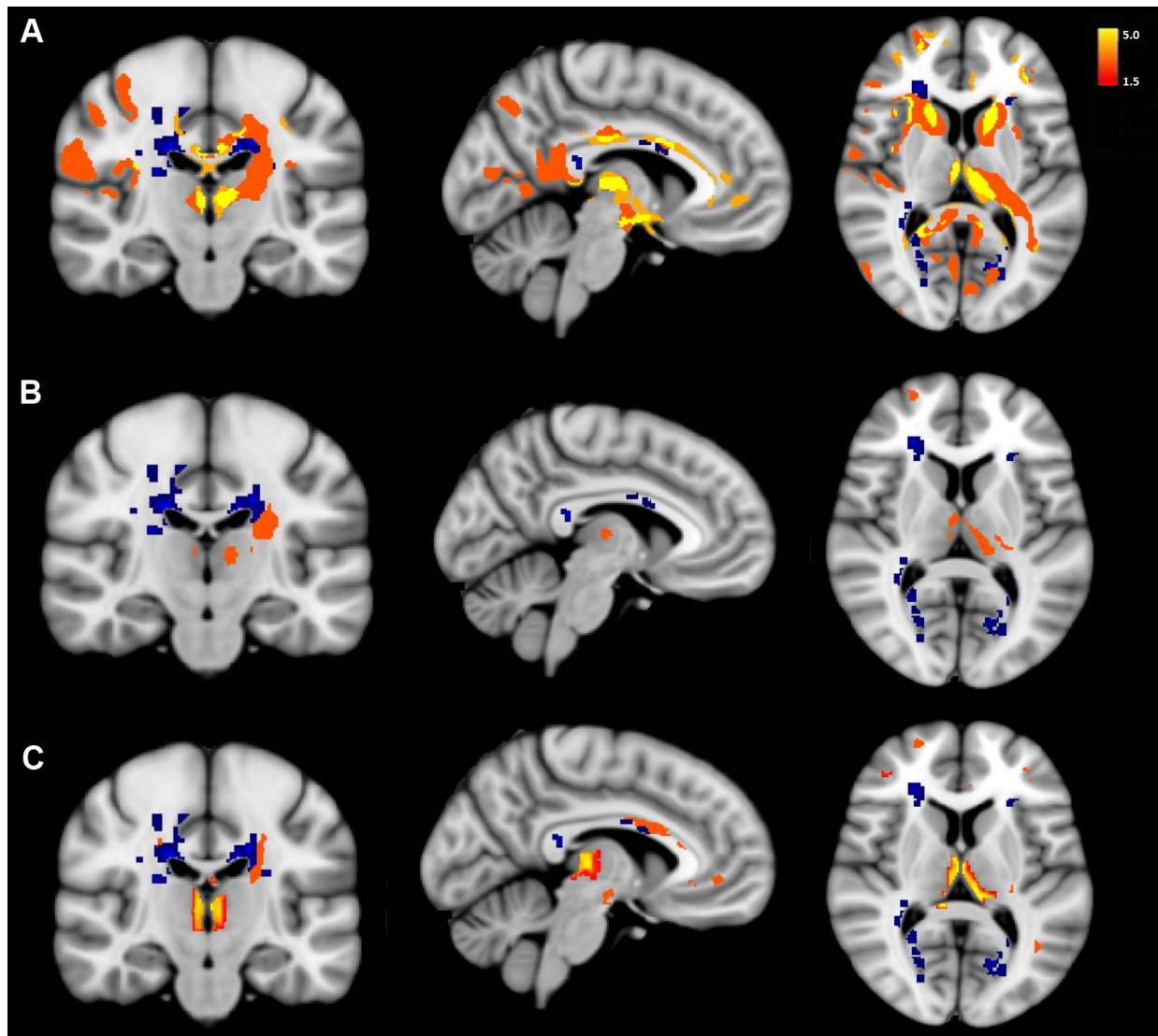


Fig. 2. Statistical parametric maps of brain sodium concentrations in MS patients. Regional increases of brain TSC (SPM8, 2-group ANCOVA $p < 0.001$, $k = 20$ voxels, corrected for FWE at a p value of 0.05) and ISC, as well as ISVF decreases (SPM8, 2-group ANOVA $p < 0.05$, $k = 10$ voxels, uncorrected for multiple comparisons) are shown respectively in A, B and C on a high-resolution T1-weighted standard template. The color bar indicates the T-scores. In blue is reported the T2 lesion probability map (50%).

Global analysis of grey and white matter sodium concentration (TSC, ISC and ISVF)

Global grey matter and white matter sodium concentrations for patients and controls are shown in **Table 2** and **Fig. 3**. In both groups, TSC was higher and ISVF lower in grey matter than in white matter ($p<0.05$) while there was no difference in terms of ISC ($p>0.1$). TSC was higher in T₁ lesions than in T₂ lesions (respectively, 52.27 ± 23.9 and 37.54 ± 12.18 mM; $p<0.015$) and both TSC in T₂ lesions and T₁ lesions were higher than in white matter (respectively, 37.54 ± 12.18 vs 31.38 ± 4.03 mM, $p<0.05$ and 52.27 ± 23.9 vs 31.38 ± 4.03 mM, $p<0.01$).

Compared to healthy controls, MS patients showed higher global grey matter and white matter TSC and ISC (respectively $p<0.05$ and $p<0.01$ for TSC; $p<0.001$ for ISC) and lower global grey matter and white matter ISVF (respectively $p=0.62$ and $p<0.001$).

Table 2. Sodium concentrations in different tissue types in healthy controls and patients with MS.

	Patients with MS	Healthy controls	p values
Grey matter TSC (mM)	42.82 ± 5.17	40.26 ± 2.99	p<0.05
Grey matter ISC (mM)	13.96 ± 1.44	13.59 ± 1.26	p<0.001
Grey matter ISVF (%)	84.20 ± 1.57	84.79 ± 1.25	p=0.62
White matter TSC (mM)	31.38 ± 4.03	27.88 ± 2.55	p<0.01
White matter ISC (mM)	14.29 ± 1.35	13.84 ± 1.26	p<0.001
White matter ISVF (%)	87.91 ± 1.52	89.38 ± 1.40	p<0.001

Data presented are mean ± standard deviation. TSC= tissue sodium concentration; ISC= intracellular sodium concentration; ISVF= intracellular sodium volume fraction

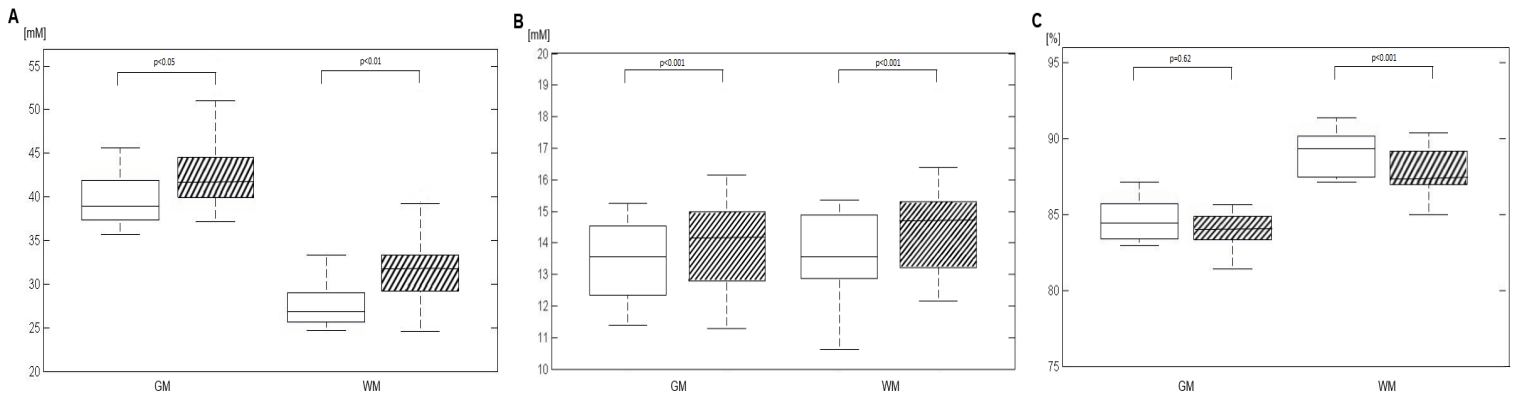


Fig. 3. Box plots displaying the 25% to 75% values (boxes) \pm 95% values (whiskers), median values (horizontal lines within boxes) of mean TSC (A), ISC (B) and ISVF (C) value distribution in grey matter and white matter among healthy controls (empty box) and patients with relapsing-remitting MS (hatched box).

Regional analysis of grey and white matter sodium concentration (TSC, ISC and ISVF)

Between-groups statistical mapping analyses performed on sodium maps are displayed in **Fig. 2**. The voxel-based analysis of grey matter showed clusters of increased TSC values in bilateral thalamus, left caudate, right anterior cingulate gyrus (BA24, BA25 and BA32), left posterior cingulate gyrus (BA23), left middle frontal gyrus (BA10), right precentral gyrus (BA6), right postcentral gyrus (BA40), ($p < 0.001$ $K_e = 20$, family wise error corrected $p < 0.05$) (**Table 3**). A voxel by voxel comparison of ISVF and ISC values within significant grey matter TSC clusters, showed lower ISVF values in portions of bilateral thalamus, right anterior cingulate gyrus (BA25 and BA32), left middle frontal gyrus (BA10), right precentral gyrus (BA6), right postcentral gyrus (BA40), ($p < 0.05$, $K_e = 10$, uncorrected for multiple comparisons) (**Table 4**) and higher ISC values in bilateral thalamus, left middle frontal gyrus (BA10), right precentral gyrus (BA6) ($p < 0.05$, $K_e = 10$, uncorrected for multiple comparisons) (**Table 5**).

The voxel-based analysis of white matter showed clusters of increased TSC values in bilateral cortico-spinal tract, bilateral anterior thalamic radiation, corpus callosum, bilateral inferior fronto-occipital fasciculus, forceps minor, uncinate fasciculus ($p < 0.001$ $K_e = 20$, family wise error $p < 0.05$) (**Table 3**). A voxel by voxel comparison of ISVF and ISC values within significant white matter TSC clusters, showed lower ISVF values in the bilateral corticospinal tract and forceps minor ($p < 0.05$, $K_e = 10$, uncorrected for multiple comparisons) (**Table 4**) and higher ISC values in left cortico-spinal tract and forceps minor ($p < 0.05$, $K_e = 10$, uncorrected for multiple comparisons) (**Table 5**).

In the restricted analysis of ISC and ISVF maps in TSC significant clusters, no cluster survived the family-wise error correction (because 133 independent voxels comparisons were tested, an adjusted significance level of 0.0004 would have granted significant results at $p < 0.05$ after multiple comparisons); therefore, for ISC and ISVF we report uncorrected results.

No clusters of decreased TSC were identified in MS patients.

Table 3. Brain regions showing an increase in TSC in MS patients compared to healthy controls.

Cluster extent	T value	MNI coordinates (mm)			Brain region	BA
		x	y	z		
4507	4.67	-9	-30	3	Left thalamus	-
	4.65	10	-30	3	Right thalamus	-
	4.13	-7	-28	3	Left anterior thalamic radiation	-
	3.80	7	-27	4	Right anterior thalamic radiation	-
3724	3.52	4	7	52	Right precentral gyrus	6
	3.52	4	12	55	Right superior frontal gyrus	6
	3.44	4	9	49	Right cingulate gyrus	24
3504	3.58	-4	-22	28	Left post cingulate cortex	23
	3.53	-6	-31	24	Corpus callosum, splenium	-
	3.47	-10	-15	31	Corpus callosum, body	-
3434	3.57	-24	-27	25	Left cortico spinal tract	-
	3.57	-30	-48	13	Left anterior thalamic radiation	-
	3.55	22	-10	24	Right cortico-spinal tract	-
	3.42	-33	-49	13	Left inferior fronto occipital fasciculus	-
2640	3.86	-15	13	9	Left caudate, body	-
		-15	21	-1	Left caudate, head	-
		-15	10	9	Left anterior thalamic radiation	-
2456	3.61	-34	52	1	Left middle frontal gyrus	10
	3.61	-34	54	-6	Left inferior fronto occipital fasciculus	-
	3.60	-34	54	1	Forceps minor	-
	3.55	-34	54	4	Uncinate fasciculus	-
1984	3.57	10	63	-12	Forceps minor	-
	3.29	19	63	-12	Right inferior fronto occipital fasciculus	-
1790	3.49	4.5	-1.8	4.5	Right thalamus	-
	3.34	-1	-12	4	Left thalamus	-
	3.33	-1	6	-10	Right anterior cingulate gyrus	25
660	3.55	22	-10	24	Right cortico-spinal tract	-
507	3.41	6	19	42	Right anterior cingulate gyrus	32
61	3.40	67	-25	19	Right postcentral gyrus	40

SPM8 2-group ANCOVA $p < 0.001$, $K_e = 20$, family wise error corrected $p < 0.05$

TSC=total sodium concentration, BA= Brodmann area

Table 4. Brain regions showing a decrease in ISVF in MS patients compared to healthy controls-ISVF voxel based analysis on TSC significant clusters.

Cluster extent	T value	MNI coordinates			Brain region	BA
		x	y	z		
2610	2.25	-22	-22	30	Left cortico spinal tract	-
855	4.73	-28	48	20	Left middle frontal gyrus	10
773	1.88	24	57	10	Forceps minor	-
683	4.24	-14	-31	3	Left thalamus	-
598	4.31	4	-9	3	Right thalamus	-
497	3.21	44	-10	43	Right precentral gyrus	6
424	3.31	-4	20	-8	Right anterior cingulate gyrus	25
318	2.37	22.5	-13	30	Right cortico spinal tract	-
188	3.15	6	22	30	Right anterior cingulate gyrus	32
60	3.05	66	-22	19	Right postcentral gyrus	40

SPM8 2-group ANOVA $p < 0.05$, $K_e = 10$, uncorrected for multiple comparisons

ISVF= intracellular sodium volume fraction, TSC= total sodium concentration, BA= Brodmann area

Table 5. Brain regions showing an increase in ISC in MS patients compared to healthy controls-ISC voxel based analysis on TSC significant clusters.

Cluster extent	T value	MNI coordinates (mm)			Brain region	BA
		x	y	z		
1473	2.46	-25	-27	16	Left cortico spinal tract	-
344	2.05	20	58	10	Forceps minor	-
245	4.17	-12	-10	4	Left thalamus	-
204	2.90	-27	36	27	Left middle frontal gyrus	10
113	2.25	42	-10	40	Right precentral gyrus	6
91	3.31	6	-10.5	9	Right thalamus	-

SPM8 2-group ANOVA $p < 0.05$, $K_e = 10$, uncorrected for multiple comparisons

ISC= intracellular sodium concentration, TSC= total sodium concentration, BA= Brodmann area

Correlations among sodium concentrations, lesion and brain volumes and clinical parameters

T₂ lesion volume was associated with TSC in cortico-spinal tract, right anterior cingulate gyrus and right precentral gyrus (r ranging from 0.47 to 0.71; 0.05<p<0.01); and with ISVF in right postcentral gyrus (r -0.59, p<0.01) and showed a trend of correlation with ISVF in corticospinal tract (r -0.46, p=0.06).

T₁ lesion volume was associated with global grey matter ISVF (r -0.53 p<0.05) and with TSC in cortico-spinal tract, right precentral gyrus, right anterior cingulate gyrus and thalamus (r ranging from 0.50 to 0.63, 0.05<p<0.01); and with ISVF in corticospinal tract and anterior cingulate gyrus (respectively r -0.55, p<0.05 and r -0.70, p<0.01).

There was no association between global and regional TSC, ISC and ISVF and measures of brain volumes except for a trend between white matter ISVF and NGMV (r=0.42, p=0.08).

While in healthy controls age was correlated with white matter (r=0.5, p<0.05) and grey matter (r=0.73, p<0.01) TSC and with grey matter ISC (r=-0.50, p<0.05), in patients age was inversely correlated with white matter (r=-0.68, p<0.01) and grey matter (r=-0.60, p<0.01) ISC but not with ISVF and TSC values (p>0.1). Disease duration was associated with white matter TSC (r=0.63, p<0.01), white matter ISC (r=-0.67, p<0.01) and grey matter ISC (r=-0.57, p=0.01).

Finally, an association was detected between global grey matter ISVF and EDSS (r=-0.47, p<0.05).

Discussion

The present study confirms previous findings of increased TSC in grey matter, white matter and focal white matter lesions (Inglese *et al.*, 2010b; Zaaraoui *et al.*, 2012; Paling *et al.*, 2013; Maarouf *et al.*, 2014) and provides first evidence of non-invasive brain intra- and extra-cellular sodium quantification in patients with MS.

Although TSC holds promise as a clinically meaningful marker of tissue injury, it does not allow to discern between the ISC concentration that reflects metabolic cellular dysfunction and/or plasticity, and the ESC that reflects expansion of the extracellular space secondary to irreversible cellular damage or edema. Herein, we employed a newly developed, non-invasive method based on the combined use of SQ and TQF ^{23}Na to measure ISC and ESC in MS patients (Fleysher *et al.*, 2010b; Fleysher *et al.*, 2013a).

There has been a significant effort over the years, to optimize the acquisition scheme and the reconstruction technique of TQF ^{23}Na imaging and improve signal to noise ratio, spatial resolution and acquisition time (Stobbe and Beaulieu, 2005; Tanase and Boada, 2005; Fleysher *et al.*, 2010b; Matthies *et al.*, 2010; Tsang *et al.*, 2012; Fleysher *et al.*, 2013a; Madelin *et al.*, 2014; Tsang *et al.*, 2015). To date, the application of TQF ^{23}Na imaging in humans has been limited to a few case reports (Boada *et al.*, 2004; Fiege *et al.*, 2013) of patients with brain tumors that have suggested a possible role for TQF ^{23}Na MRI to discriminate cell proliferation (tumor recurrence) from areas of tumor necrosis and edema (Boada *et al.*, 2004; Fiege *et al.*, 2013). Although promising, these approaches were limited to a qualitative assessment of the pathologic tissue.

To overcome this limitation, our method combined SQ and TQF ^{23}Na MRI, to quantify TSC and the intracellular sodium molar fraction (ISMF) and then derive ISC and the ISVF, an indirect measure of ESC (the lower the ISVF, the higher the ESC) (Fleysher *et al.*, 2013a). A previous application of this

method in healthy volunteers resulted in brain ISC values between 10–15 mmol/L and an ISVF values between 85–95 %, in line with previous theoretical predictions and experimental works (Fleysher *et al.*, 2013a).

Global and regional white matter TSC, ISC and ISVF

Global white matter TSC and ISC values were higher and ISVF values lower in patients than controls supporting the concept that TSC is not only the mere consequence of the expansion of the extracellular space secondary to demyelination and neuroaxonal loss. Similar results were found at a regional level where the voxel based analysis showed not only a quite widespread ISVF decrease within the white matter clusters of increased TSC, but also a fewer clusters of ISC increase.

Since none of our patients had Gadolinium-enhancing lesions, the decrease of ISVF (i.e., ESC increase) is likely to reflect tissue disruption, demyelination and axonal loss not only within lesions but also, to a lesser extent, within normal-appearing white matter. Due to the difference in spatial resolution between the T₂-weigheted images and the TQF ²³Na images we decided to analyze the global white matter rather than normal appearing white matter. However, as reported in previous ²³Na MRI studies of patients with MS (Inglese *et al.*, 2010b; Zaaraoui *et al.*, 2012; Paling *et al.*, 2013; Maarouf *et al.*, 2014) and as visualized in Fig. 2, TSC, ISC and ISVF are altered not only in white matter areas occupied by lesions but also in white matter areas outside clusters of lesions. The lack of complete correspondence between T₂ lesion map and sites of ²³Na increases on SPM maps can be explained by the low resolution of sodium maps. The averaging of lesional and non-lesional sodium concentration in each voxel most likely prevented the voxel wise statistical analysis from identifying increased sodium concentration specifically within white matter lesions.

Several factors may explain the increase of ISC. First of all, the upregulation of voltage-gated sodium channels along demyelinated axons in lesions and normal appearing white matter leads to restoration of

conduction at the cost of an increased influx of intraxonal sodium ions (Waxman, 2006a). Second, the disease-related mitochondrial dysfunction can lead to a reduction in energy supply and to the failure of ATP-dependent pumps (Dutta *et al.*, 2006; Trapp and Stys, 2009) that further increase the intraxonal sodium concentration. Third, the intraxonal influx of Na ions can occur through persistent Na channels (Stys *et al.*, 1993; Taylor, 1993) and glutamate receptors (Ouardouz *et al.*, 2006) contributing to the intracellular accumulation and to the dysfunction of the Na/Ca exchanger. Finally, the well-established upregulation of Na channels in activated microglia, macrophages and reactive astrocytes within active and chronic MS lesions (Craner *et al.*, 2005; Black *et al.*, 2010) is likely to contribute to the measured increase of ISC. All together, these pathophysiological processes can either lead to neuroaxonal death through the increase of intracellular calcium, the activation of calcium dependent proteases, and glutamate-mediated cytotoxicity (Trapp and Stys, 2009) or to a spontaneous reverse of metabolic dysfunction into a physiological condition (Nikic *et al.*, 2011). Although it remains only a speculation due to the cross-sectional design of our study and the lack of confirmatory *post-mortem* data, we believe that the ISC increase in our relapsing-remitting MS patients reflects neuroaxonal metabolic dysfunction rather than loss. This is supported by several findings of our study: a) the association of conventional MRI measures of tissue destruction such as T₁ lesion volume and normalized grey matter volume with the decrease of ISVF but not with the increase of ISC; b) the correlation between the EDSS score and measures of ISVF decrease but not ISC increase; c) the presence of an inverse relationship of disease duration with ISC and a direct relationship with TSC and ISVF suggesting that while TSC and ISVF are expression of structural damage, which increases as the disease progresses, ISC increase could reflect a compensatory mechanism, more active in the initial stage of the disease and becoming less efficient as the disease progresses. Hence, ISC might provide information about brain areas that are metabolically dysfunctional but still able of functional compensatory mechanisms preventing structural alterations.

Global and regional grey matter TSC, ISC and ISVF

Global grey matter TSC and ISC values were higher in patients than controls while the difference in ISVF did not reach a statistical relevant difference although the values were lower in MS patients. Similarly to the white matter regional analysis, a decrease in ISVF was detected in almost all the cortical and deep grey matter regions that showed a TSC increase, while ISC increase was detected only in a few areas.

Our findings about the regional brain distribution of increased TSC are in agreement with those of a previous study in relapsing-remitting MS (Zaaraoui *et al.*, 2012), that showed increased TSC in areas involved in locomotor function (left caudate, right premotor cortex) as well as areas involved in high cognitive functions, speech, stimuli integration and emotion (thalamus, cingulate cortex, bilateral prefrontal cortex, right postcentral gyrus). The presence of cortical grey matter lesions may explain changes in both ISVF and ISC. Cortical lesions are a very frequent finding at histological examination of brain samples (Kutzelnigg *et al.*, 2005) and a quite common finding in patients with MS when non-conventional MRI sequences such as double inversion and phase sensitive inversion recovery are employed. Neuronal loss can be very extensive in cortical lesions and can lead to the increased TSC found in the grey matter of our patients. However, in patients with relapsing-remitting MS cortical lesions are less frequent than in patients with progressive MS and they are characterized by demyelination rather than axonal loss (Kutzelnigg *et al.*, 2005). Thus, explaining the relevant increase of ISC in presence of a less conspicuous change in global ISVF.

Nevertheless, ISVF was decreased in grey matter clusters of increased TSC suggesting that, in addition to cortical lesions, other mechanisms can lead to neuroaxonal loss in the cortex. Indeed, it has been shown that grey matter damage occurs as a consequence of trans-synaptic degeneration of axons transected in distant white matter lesions and/or secondary to the diffuse microscopic damage occurring

in normal appearing white matter (Sailer *et al.*, 2003; Bodini *et al.*, 2009). Pro-inflammatory and cytotoxic mediators derived from the meninges may also have a direct pathological effect on normal-appearing, non demyelinated grey matter as suggested by recent *post-mortem* and in vivo PK11195 PET studies (Magliozzi *et al.*, 2010; Politis *et al.*, 2012).

In addition to the redistribution of sodium channels in demyelinated cortical lesions, cortical mitochondrial dysfunction can contribute to the increase of intracellular sodium. Campbell and colleagues have demonstrated the presence of respiratory-deficient neurons with multiple mitochondrial DNA deletions or absence of catalytic subunits of complex IV in layer VI of the cortex of brain samples from patients with MS (Campbell *et al.*, 2011).

Our findings in the grey matter have to be interpreted with caution due to the spatial resolution of our triple-filtered ^{23}Na scans. We tried to minimize partial volume effect by using a 0.5 probability (rather than the more commonly used 0.75) as a threshold for grey and white matter tissue type classification. However, we cannot rule out that the inclusion of voxels containing in part cerebro-spinal fluid and white matter may have biased the grey matter measures. Future improvement in MRI acquisition techniques and coil design will lead to smaller voxel sizes and more accurate measurements.

Several limitations have to be considered when interpreting our results. First, we focused on patients with relapsing-remitting MS and on a cross-sectional design study to determine the feasibility of our method; future longitudinal studies, designed to follow over time patients with different clinical subtypes will allow to extend our investigation on the clinical impact of sodium concentration increase in the transitional stage between relapsing and progressive phases of the disease. Second, due to the inherently low signal of TQF ^{23}Na , we selected larger voxel size that precluded a reliable assessment of ISVF and ISC within white matter lesions. Future implementations of our technique and the use of multichannel receive arrays for sodium imaging will improve image SNR and will allow the voxel size

to be reduced, thus improving the accuracy and precision of concentration quantification in white matter lesions.

Third, the application of our model in MS is based on the assumption that the pathology itself does not determine any substantial, persistent, alteration of ^{23}Na relaxation times. Nonetheless, the specific effect of microstructural alterations on ^{23}Na relaxation times has not been ruled out and the possibility of protein induced alteration of ^{23}Na relaxation times cannot be excluded (Bansal *et al.*, 2000).

Fourth, as this was an exploratory study, correction for multiple comparisons was not performed; however, all analyses were performed with established a priori hypotheses. Correction for family-wise error was only applied to the whole brain voxel wise comparison of TSC maps to avoid a massive multiple comparison problem.

Finally, even if a correction for B1 inhomogeneity was applied, we cannot exclude the presence of residual radiofrequency field artifacts. In addition, possible contribution to TQF signal from the extracellular sodium could have biased the results of the measurement. Although the intracellular origin of the TQF signal is supported by studies in experimental models (Winter and Bansal, 2001), it is not possible to clarify the magnitude of the bias, if any, based on the tissue model and the acquisition used in this work. We believe, however, that since ISC and ISVF values obtained in our study (Fleysher *et al.*, 2013a) were within the expected physiological range, the possible biases remained small. Future studies comparing ours with new models and acquisition schemes (Stobbe and Beaulieu, 2005; Madelin *et al.*, 2014) will help clarify this issue.

Although preliminary, our findings demonstrate that TQF ^{23}Na MRI is feasible in patients with MS and that ISC and ISVF values can complement TSC measures by providing information about different pathophysiologic aspect of MS. ISVF values reflect expansion of the extracellular volume related to cellular loss and development of tissue atrophy; ISC values reflect changes in cellular metabolism

related to mitochondrial and ion channels dysfunction. Abnormal cellular metabolism and ion dyshomeostasis can either lead to cellular death or can reverse to physiological conditions. Hence, ISC may be a potential tool for the selection of patients with brain neuroplastic reserve and repair capability who may benefit from preventive neuroprotective treatments before the occurrence of structural damage (Kapoor, 2006; Nikic *et al.*, 2011; Arun *et al.*, 2013). Future improvements in ^{23}Na MRI acquisition (Matthies *et al.*, 2010), reconstruction algorithms and coil design as well as the employment of alternative approaches (Madelin *et al.*, 2014) are needed to understand the dynamics of sodium changes in the different stages of the disease and their clinical impact.

PART 3

Brain intracellular sodium concentration:

A window on age-related microstructural changes

Introduction

Post mortem studies and MR investigations have extensively characterized the brain structural modifications associated to normal aging, disclosing the presence of both morphological changes and micro- structural damage (Rees, 1976; Meier-Ruge *et al.*, 1992; Kemper, 1994; Tang *et al.*, 1997; Marner *et al.*, 2003; Hedman *et al.*, 2012; Billiet *et al.*, 2015). Topographic distribution and temporal evolution pattern of such modifications seem to be tissue specific: while grey matter volume (GMV) shows a linear decline with age (Sowell *et al.*, 2004; Raz and Rodrigue, 2006; Giorgio *et al.*, 2010b), white matter volume (WMV) evolution is more controversial (Good *et al.*, 2001; Ge *et al.*, 2002; Benedetti *et al.*, 2006). It seems to remain steady or increase slowly through adulthood, due to the ongoing maturational processes, peaks around the 4th decade and subsequently declines, unevenly across brain regions, from the 6th decade onward (Guttmann *et al.*, 1998; Salat *et al.*, 1999; Courchesne *et al.*, 2000; Bartzokis *et al.*, 2001; Jernigan *et al.*, 2001; Ge *et al.*, 2002; Liu *et al.*, 2003; Allen *et al.*, 2005; Fotenos *et al.*, 2005; Walhovd *et al.*, 2005; Pagani *et al.*, 2008; Giorgio *et al.*, 2010a; Kakimoto *et al.*, 2016). Microstructurally, the simplification of dendrite arborization, degeneration of myelin sheaths, reduced synaptic and fiber density induce modification in the tissue myelin content and diffusivity properties that can be explored through specific imaging modalities (e.g. diffusion tensor imaging-DTI and magnetization transfer imaging-MTI) (Abe *et al.*, 2002; Pfefferbaum *et al.*, 2005; Salat *et al.*, 2005; Benedetti *et al.*, 2006; Ota *et al.*, 2006; Sullivan *et al.*, 2006; Abe *et al.*, 2008). Although sensitive to the effects of aging, often these modalities are not specific to any underlying biological mechanism or to the specific electrophysiological changes occurring with aging (Rizzo *et al.*, 2014). Among the latter, studies in animal models have reported age-related changes in the action potential characteristics, with increased threshold and decreased amplitude, possibly linked to alterations of sodium (²³Na) channel activation properties (Randall *et al.*, 2012). Altered expression of

^{23}Na channel subtypes and reduced expression of ^{23}Na channels, resulting from changes in myelin sheath organization, have also been reported (Boiko *et al.*, 2001).

^{23}Na yields the second strongest nuclear magnetic resonance (NMR) signal among all biologically relevant NMR-active nuclei but the concentration of ^{23}Na ions in the human body is much lower than the ^1H concentration; in addition, ^{23}Na MRI presents a poor signal to noise ratio, which is responsible for the long acquisition time and the poor spatial resolution of ^{23}Na MRI in comparison with standard ^1H MRI. While quantification of tissue total sodium concentration (TSC) can be achieved through single quantum (SQ) ^{23}Na MRI (Inglese *et al.*, 2010a), the determination of intracellular sodium concentration (ISC) requires the application of higher magnetic fields and more advanced imaging techniques (Stobbe and Beaulieu, 2005; Fleysheer *et al.*, 2010a; Tsang *et al.*, 2012; Fleysheer *et al.*, 2013b; Madelin *et al.*, 2014; Tsang *et al.*, 2015). Recently, we have implemented a new pulse sequence for the acquisition of triple quantum ^{23}Na MRI at 7 Tesla (T) (Fleysheer *et al.*, 2010a) and we have applied to a small cohort of MS (MS) patients a newly developed method that combines SQ and TQF ^{23}Na MRI to assess ISC and intracellular sodium volume fraction (ISVF), an indirect measure of extracellular sodium concentration (ESC) (Petracca *et al.*, 2016). Our results suggest that, while ISVF reflects the presence of tissue loss and expansion of extracellular space, ISC increase could reflect neuro-axonal metabolic dysfunction related to mitochondrial and ion channels dysfunction (Petracca *et al.*, 2016). ISC exploration could therefore allow a non-invasive assessment of the aging brain metabolic state, contributing to the clarification of the mechanisms underlying the aging process and providing a baseline for comparison of brain abnormalities that occur during the preclinical stage of neurological disorders, especially those whose risk increases with advancing age (e.g. dementia).

In this study, investigating the relationship between age, morphologic changes expressed by brain volumes and microstructural modifications expressed by ^{23}Na concentrations, we aimed to (i)

demonstrate how ^{23}Na MRI could contribute valuable information on age-related microstructural changes and (ii) provide normative data on ^{23}Na concentrations for future studies.

Material and methods

Subjects

MRI data were acquired in a group of 45 healthy subjects. Exclusion criteria were a previous history of psychiatric or neurological disease, substance abuse and the presence of MRI abnormalities such as infarct, vascular malformation or tumors. Informed written consent was obtained from all participants according to ethical approval from the NYU Research Ethics Committee.

MRI acquisition

All subjects underwent ^1H MRI at 3 T (Siemens Medical Solutions) and SQ and TQF ^{23}Na MRI at 7 T (MAGNETOM, Siemens Healthcare).

The 3 T ^1H MRI protocol included the following sequences: (i) dual-echo turbo spin echo (repetition time = 8000 ms, echo time = 11 ms, 45 contiguous 3-mm thick axial slices); (ii) 3D T1-weighted magnetization-prepared rapid-acquisition gradient echo (repetition time = 2300 ms, echo time = 2.98 ms, inversion time = 900 ms, flip angle = 9° , voxel size = 1 mm^3).

The sodium SQ and TQF protocol at 7 T was acquired with a custom-built dual-tuned TX/RX $^1\text{H}/^{23}\text{Na}$ head coil (Wiggins *et al.*, 2010).

SQ ^{23}Na MRI was acquired using a 3D gradient echo sequence (repetition time = 150ms, echo time = 6.8 ms, flip angle = 90° , field of view = $240 \times 240\text{mm}^2$, matrix = 48×48 , voxel size = $5 \times 5 \times 5\text{ mm}^3$); TQF ^{23}Na MRI was acquired using a modified 3D gradient-echo sequence with a new 12- step phase-cycling B0-corrected TQF scheme (repetition time = 150 ms, echo time = 6.8 ms, flip angle = 90° , field of view = $240 \times 240 \times 240\text{ mm}^3$, matrix $30 \times 30 \times 24$, voxel size $8 \times 8 \times 10\text{mm}^3$, $\tau_1 = 6.8\text{ ms}$ $\tau_2 = 150\text{ ms}$, two averages) (Fleysher *et al.*, 2013b). For the purposes of TSC quantification, calibration phantoms with known sodium concentrations (50 and 100mM/l) were placed into the field of view. For

TQF B0 correction, B0 maps were computed from the phase difference between two SQ images acquired over 3.6 min (repetition time = 150 ms) with echo times = 6.8 ms and 8.8 ms, respectively. The SQ image with echo time = 6.8 ms was used for TSC calculation. B1 maps were computed from the ratio of two additional SQ images acquired over 3.6 min with fractional anisotropy = 60 and 120, repetition time = 150 ms using the double flip angle method. Using the B1 maps, B1 correction was applied to SQ and TQF images (Fleysher *et al.*, 2013b).

Image processing

When present, white matter hyperintensities (WMHs) were identified and outlined on the dual-echo images using a semi-automated technique based on user-supervised local thresholding (Jim version 6; Xinapse Systems, <http://www.xinapse.com>) in order to quantify their volume. Normalized brain volume (NBV), GMV and WMV) were computed for all subjects on the 3D T1-weighted sequence using FSL's SIENAX program (SIENAX; FMRIB Centre, Oxford, UK) as described elsewhere (Battaglini *et al.*, 2012).

As previously described (Fleysher *et al.*, 2013b), ISC and ISVF were quantified as follows. First, SQ and TQF images were acquired and corrected for B0 and B1 inhomogeneities as described in Fleysher *et al.* (2010). Second, TSC maps were quantified in Image J v.1.36b on a voxel-by-voxel basis from the SQ images using a linear method, dependent on the calibration phantom, as described by Inglese *et al.* (2010). Third, SQ and TQF images were combined with TSC maps using an in-house procedure developed in Matlab (Fleysher *et al.*, 2013b) and ISC and ISVF maps were computed. The resulting concentration maps were further analyzed with a global approach to measure TSC, ISC and ISVF over the entire grey and white matter (GM, WM) tissue.

The analysis of the ²³Na concentration maps (i.e. TSC, ISC and ISVF maps) was performed with FSL 5 (<http://fsl.fmrib.ox.ac.uk/fsl/fslwiki>). The TSC maps were co-registered to the corresponding T1-

weighted images with an affine-linear registration and the transformation matrices were saved. T1-weighted images were segmented and the obtained GM and WM masks were superimposed onto ^{23}Na concentration maps in native ^{23}Na -image space using the inverse transformation matrix obtained in the step above; mean values from each tissue were extracted for each subject, obtaining GM, WM and cerebrospinal fluid TSC, ISC and ISVF values. A probability of 50% was considered as threshold for GM and WM tissue type classification. Whole brain (WB) ^{23}Na concentrations were computed applying the following formula: $(^{23}\text{Na concentration WM} * \text{WMV}) + (^{23}\text{Na concentration GM} * \text{GMV}) / (\text{GMV} + \text{WMV})$.

Statistical analysis

Statistical analysis was performed using SPSS 22.0 (SPSS, Chicago, IL). In order to provide age-related normative values for ^{23}Na concentrations we divided subjects into young adults (YA), middle-aged adults (MA) and older adults (OA). The ages chosen for defining the different age subgroups are broadly consistent with previous studies (Salat *et al.*, 2005; McLaughlin *et al.*, 2007; Giorgio *et al.*, 2008). Group comparisons were performed with Chi-squared Test and ANOVA, as appropriate. Since age related changes in brain morphology exhibit sex specificity (Good *et al.*, 2001; O'Dwyer *et al.*, 2012; Kakimoto *et al.*, 2016), sex was entered as covariate in the ANOVA analysis.

Relationships between brain structure (volumes and ^{23}Na concentrations) and age were explored both linearly and non-linearly with a hierarchical regression analysis, using age and age² as regressors.

Annual rates of change were calculated from the slope of the regression line (volume or ^{23}Na metrics versus age at assessment), dividing the slope by the intercept in order to provide a percentage annual variation value that could be compared across the various metrics.

To compare the linear and non-linear approaches, regression plots were produced to visually assess the best fitting. Subsequently, to take into account the effect of sex and other potentially confounding variables on the relationship between age and ^{23}Na concentrations, we repeated the correlation analysis entering sex, brain volumes and WMHs as covariates. Partial correlations between ^{23}Na concentrations and brain volumes were also tested, entering sex and WMHs as covariates. Statistical significance was set at a p value ≤ 0.05 .

Results

Demographic and structural features

Twelve out of 45 enrolled subjects (29 males, 16 females, median age=43.2 years, range=19.6-76.9 years) presented non-specific WMHs (27%). For the purpose of subsequent subgroup analyses, subjects were further classified into YA (n=21, 13 males, 8 females, median age=30.6, range=19.6-39.9 years), MA (n=16, 11 males, 5 females, median age=50.8, range=40.1-59.6 years) and OA (n=8, 5 males, 3 females, median age=64.8, range=61.6-76.9 years). No difference in term of sex was detected between groups (p= 0.90). Structural MR features of the three groups are reported in **Table 1**. Brain volumes and ²³Na concentrations significantly differed among age groups, with the exception of WM TSC and WM ISVF (respectively p= 0.06 and p= 0.07) (**Table 1**). Annual percentage variations for all the explored variables are reported in **Table 2**.

Table 1. Structural MR features.

	YA	MA	OA
WMHs, mL	0.25 (0.72)	0.80 (2.97)	1.74 (2.05)
NBV, mL	1565.90 (49.09)	1505.43 (46.39)	1458.25 (77.73)**
GMV, mL	821.66 (25.83)	771.18 (41.76)	748.25 (37.51)**
WMV, mL	749.09 (41.75)	734.12 (37.73)	710 (62.56)**
TSC WB, mM	31.57 (2.43)	33.86 (2.39)	35.66 (3.04)**
TSC GM, mM	36.74 (3.51)	40.01 (3.31)	42.74 (3.41)**
TSC WM, mM	25.86 (1.67)	27.34 (2.56)	28.18 (3.11)
ISVF WB, %	87.70 (1.07)	87.09 (0.90)	86.00 (1.00)**
ISVF GM, %	85.60 (1.32)	84.79 (1.13)	83.33 (0.93)**
ISVF WM, %	89.99 (1.25)	89.53 (1.07)	88.81 (1.20)
ISC WB, mM	14.50 (1.71)	13.59 (1.64)	13.23 (0.72)*
ISC GM, mM	14.42 (1.69)	13.45 (1.60)	13.07 (0.83)**
ISC WM, mM	14.57 (1.75)	13.72 (1.72)	13.39 (0.69)**

All values express mean (SD). * $p < 0.05$, ** $p < 0.01$ ANOVA, sex corrected

Abbreviations: YA= young adults, MA= middle-aged adults, OA= older adults, NBV= normalized brain volume, GMV= grey matter volume, WMV= white matter volume, WM= white matter, WMHs = white matter hyperintensities, TSC= total sodium concentration, WB= whole brain, GM= grey matter, ISVF= intracellular sodium volume fraction, ISC= intracellular sodium concentration.

Table 2. Percentage annual variation.

NBV	GMV	WMV	TSC WB	TSC GM	TSC WM	ISVF WB	ISVF GM	ISVF WM	ISC WB	ISC GM	ISC WM
-0.18	-0.21	-0.15	0.35	0.45	0.25	-0.04	-0.06	-0.03	-0.26	-0.27	-0.25

Abbreviations: NBV= normalized brain volume, GMV= grey matter volume, WMV= white matter volume, TSC= total sodium concentration, WB= whole brain, GM= grey matter, WM= white matter, ISVF= intracellular sodium volume fraction, ISC= intracellular sodium concentration.

Regression analyses across the whole group

Linear and non-linear regression results are reported in **Table 3**. While all brain structural metrics showed a linear relationship with age, no quadratic relationship was disclosed by the non-linear regression analysis (**Fig. 1** and **Fig. 2**). After correcting for sex, brain volumes and WMHs, correlations between age and ISC were confirmed (WB $r = -0.37$, $p < 0.05$; GM $r = -0.32$, $p < 0.05$; WM $r = -0.40$, $p < 0.01$) while none of the correlations between age and ISVF reached the statistical significance (WB $r = -0.07$, $p = 0.65$; GM $r = -0.23$, $p = 0.13$; WM $r = -0.25$, $p = 0.11$). The relationship between age and TSC survived only in the WM compartment (WB $r = 0.21$, $p = 0.18$; GM $r = 0.27$, $p = 0.09$; WM $r = 0.41$, $p < 0.01$). No significant correlations were identified between WMV and sodium concentrations (TSC $r = -0.16$, $p = 0.32$; ISVF $r = 0.23$, $p = 0.14$; ISC $r = -0.12$, $p = 0.43$) while GMV was significantly correlated with GM TSC ($r = -0.60$, $p < 0.01$) and GM ISVF ($r = 0.51$, $p < 0.01$) but not with GM ISC ($r = 0.17$, $p = 0.28$).

Table 3. Parameter estimates of regressor equations for the linear and non-linear (quadratic) effects of age on brain volumes and sodium concentrations.

	Linear				Non-linear		
	R Square	β	F	p	R Square	F	p
WMHs	0.13	0.36	6.41	0.01	0.02	0.86	0.36
NBV	0.44	-0.66	33.93	<0.01	0.01	0.57	0.45
GMV	0.43	-0.66	33.00	<0.01	0.00	0.08	0.78
WMV	0.13	-0.36	6.29	<0.05	0.01	0.63	0.43
TSC WB	0.27	0.52	15.89	<0.01	0.00	0.13	0.72
TSC GM	0.29	0.54	17.93	<0.01	0.01	0.49	0.49
TSC WM	0.13	0.37	6.70	0.01	0.00	0.04	0.85
ISVF WB	0.24	-0.49	13.55	<0.01	0.02	0.71	0.40
ISVF GM	0.27	-0.52	15.83	<0.01	0.00	0.15	0.70
ISVF WM	0.11	-0.33	5.15	<0.05	0.02	1.06	0.31
ISC WB	0.14	-0.38	7.11	0.01	0.00	0.18	0.67
ISC GM	0.15	-0.39	7.78	<0.01	0.00	0.15	0.70
ISC WM	0.12	-0.35	6.08	<0.05	0.00	0.20	0.66

Abbreviations: WMHs = white matter hyperintensities, NBV= normalized brain volume, GMV= grey matter volume, WMV= white matter volume, WM= white matter, TSC= total sodium concentration, WB= whole brain, GM= grey matter, ISVF= intracellular sodium volume fraction, ISC= intracellular sodium concentration.

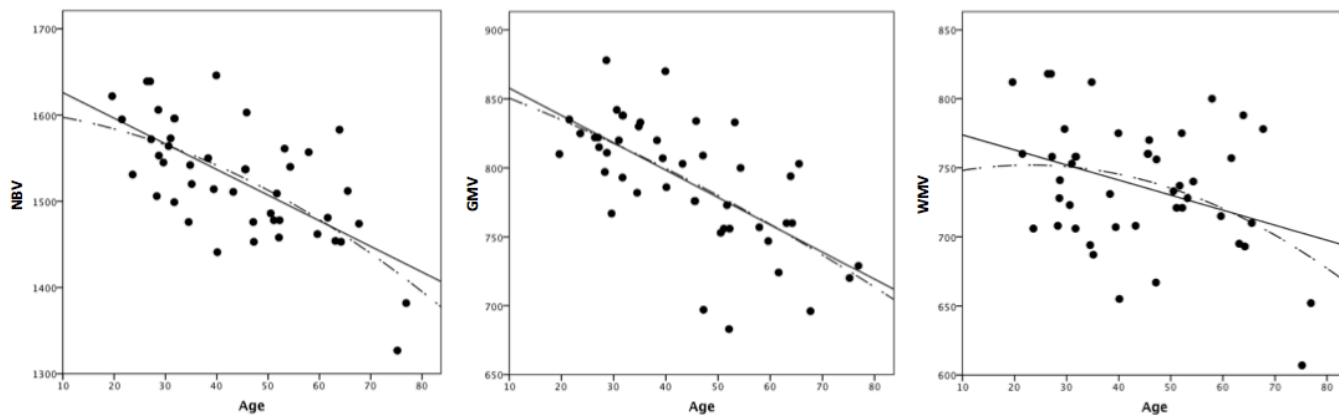


Fig. 1. Regression plots between age and brain volumes (i.e., normalized brain volume [NBV], gray matter volume [GMV], and white matter volume [WMV]) for the linear (continuous line) and quadratic (dotted line) models.

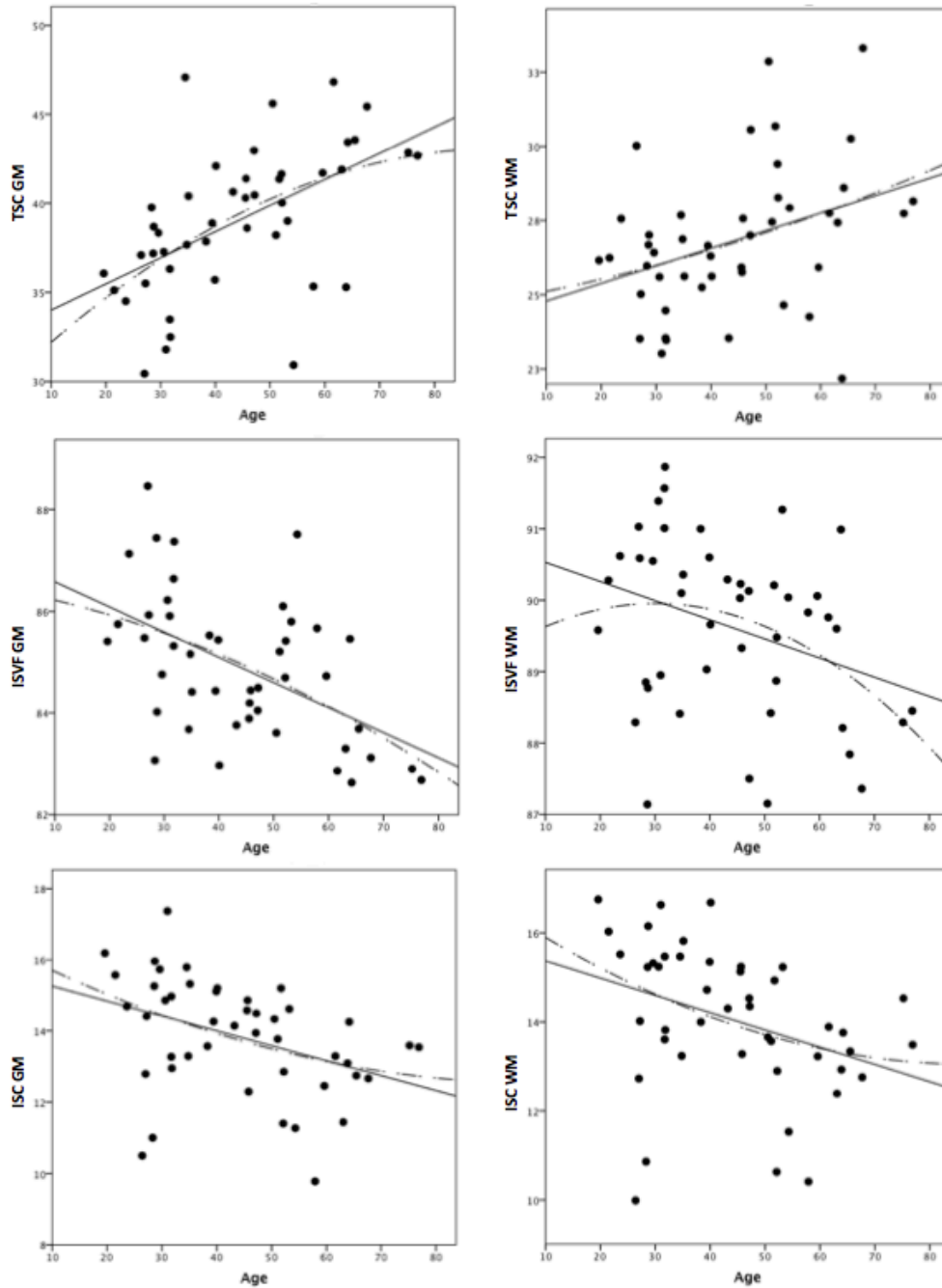


Fig. 2. Regression plots between age and ^{23}Na metrics (i.e., total sodium concentration [TSC], intracellular sodium volume fraction [ISVF] and intracellular sodium concentration [ISC]) for the linear (continuous line) and quadratic (dotted line) models used to assess the gray matter and white matter compartments.

Discussion

In the present cross-sectional study, applying TQF ^{23}Na MRI to a cohort of healthy adults, we provide for the first time normative data for ^{23}Na concentrations in three age groups (<40, 40-60, >60). Our main objective, however, was to clarify the role of ISC in the characterization of tissue microstructural abnormalities occurring with aging. To this purpose, we explored the relationship between ^{23}Na concentrations (TSC, ISC and ISVF), brain volumes and age in 45 healthy subjects. TSC showed a linear increase with age, while brain volumes exhibited a constant decline, associated with the expansion of the ECS (ISVF decrease) but not with ISC decrease. According to the canonical brain-sodium tissue model, ^{23}Na is distributed between only two compartments: intracellular and extracellular (Thulborn *et al.*, 1999b; Ouwerkerk *et al.*, 2003). While TSC represents an average of the two compartments, ISVF is an indirect measure of ESC and therefore is sensitive to the detection of neuro-axonal loss, as confirmed by our previous findings in MS patients (Petracca *et al.*, 2016) and by the correlation between ISVF and GMV detected in the present study. *Postmortem* assessment and MR studies of brain tissue have revealed increased axonal dispersion (Meier-Ruge *et al.*, 1992) and loss of small diameter myelinated fibers (Tang *et al.*, 1997; Marner *et al.*, 2003) with age, resulting in an increased amount of interstitial fluid that can explain the observed ISVF decrease in brain tissue with age. On the other hand, our finding of an age-related decrease in ISC, independent from brain volumes reduction, suggests how ISC might be able to depict modifications in neuronal morphology and ^{23}Na channel expression induced by aging, providing valuable and specific information on tissue microstructure. In particular, ISC decrease could be related to the reduction in the complexity of dendrite arborization, change in synaptic densities due to reduction in spine number, myelin sheaths disruption and reduced expression/altered functionality of ^{23}Na channels occurring with age (Dickstein *et al.*, 2007; Rizzo *et al.*, 2014). To further confirm this hypothesis we tested the correlation between age and ^{23}Na concentrations taking into account the presence of WMHs and brain volumes. As

expected, only the correlation between ISC and age was still significant, reinforcing the idea that the changes depicted by ISC are independent from neuro-axonal loss and atrophy. While for brain volumes loss a different temporal kinetic is usually reported, with GMV loss occurring earlier than WMV reduction, data about the temporal dynamic of microstructural modifications in GM are scarce, mainly because so far studies exploring microstructural tissue modifications in aging have focused on WB or WM analysis (Hofman *et al.*, 1999; Rovaris *et al.*, 2003; Pfefferbaum *et al.*, 2005; Abe *et al.*, 2008; Barrick *et al.*, 2010; Giorgio *et al.*, 2010a; O'Dwyer *et al.*, 2012; Sala *et al.*, 2012; Billiet *et al.*, 2015); however, the few available data suggest that brain WM and GM have different vulnerabilities to aging (Benedetti *et al.*, 2006). In agreement with this hypothesis, the value of the correlation coefficient between brain volumes and age was higher for the GM than for the WM, and age explained three times more of the variance in GM than in WM tissue volume. In our population, both GM and WM volumes loss appears linearly related to age, and WMV does not exhibit the quadratic relationship with age mainly reported in literature, with a first wave of growth occurring from childhood to age 13 and a second wave of growth/stability occurring from adolescence to age 35 (Hedman *et al.*, 2012), possibly because our sample did not include child or adolescents and less than 40% of our sample was aged <35 years.

²³Na concentrations also exhibited a linear relation with age, suggesting that microstructural modifications occur since the early adulthood and then proceed constantly throughout the lifespan. The relationship between ²³Na concentrations and age showed the same temporal dynamic in GM and WM, but the between group comparison hinted to a different degree of involvement of the two tissues: the lack of significant difference for WM TSC and ISVF in the between group comparison suggests that age-related tissue modifications might affect WM to a lower extent than GM. The percentage annual variations of ²³Na concentrations seem to confirm this hypothesis, since WM TSC, ISC and ISVF percentage annual variations are lower in the WM compartment than in the GM. While this finding

seems to confirm a prevalent involvement of GM in age related changes, the discrepancy between the two compartments could also be attributed to the lack of specificity of ^{23}Na metrics towards myelin modifications. In future studies, the integration of ^{23}Na imaging with other imaging modalities could help clarify this point and characterize the different aspects of tissue microstructural changes ongoing in the gray and white matter compartments with age. The parallel analysis of ^{23}Na concentrations and metrics derived from other MR modalities could also contribute to the biological interpretation of metrics that, although lacking in specificity, are still widely used in clinical studies. For example, the decrease in the DTI derived metric fractional anisotropy (FA) observed during aging could be related to changes in myelin content and/or increased axonal dispersion (Billiet *et al.*, 2015); the latter interpretation could find further confirmation in an association between FA and ISVF. Several limitations have to be considered when interpreting our results. First, our population did not include children or adolescents and therefore our study does not capture the evolution of ^{23}Na concentrations across the entire lifespan. Second, since we did not explore topographic patterns of ^{23}Na concentrations regionally, we cannot infer whether the observed changes occur uniformly across the brain or are localized to particular brain regions, as would support the frontal-aging hypothesis (West, 1996). Finally, due to the nature of our study, we did not examine the rate of change in ^{23}Na parameters longitudinally.

In conclusion, although our interpretation remains speculative due to the lack of *postmortem* histologic verification, we believe that ISC reflects neuro-axonal metabolic state rather than loss. This is supported by (i) the association of GMV with ISVF but not with ISC (since ISVF decrease is expression of extracellular space expansion, its direct correlation with GMV is to be expected); (ii) the association of ISC, but not ISVF with age after correction for sex, brain volumes and WMHs. Future studies exploring longitudinally ^{23}Na metrics in association with other imaging modalities will help elucidate the dynamics of ^{23}Na changes with age and their biological role.

Copyright acknowledgment

Part 1 Reproduced from Petracca et al. Sodium MRI of MS. *NMR Biomed.* 2016 Feb; 29(2): 153-61 by permission of John Wiley & Sons, Ltd (license number 3835580803143).

Part 2 Reproduced from Petracca et al. Brain intra- and extracellular sodium concentration in MS: a 7 T MRI study. *Brain.* 2016 Mar; 139(Pt 3): 795-806 by permission of Oxford University Press (license number 3835580383008).

References

- Abe O, Aoki S, Hayashi N, Yamada H, Kunimatsu A, Mori H, *et al.* Normal aging in the central nervous system: quantitative MR diffusion-tensor analysis. *Neurobiol Aging* 2002; 23(3): 433-41.
- Abe O, Yamasue H, Aoki S, Suga M, Yamada H, Kasai K, *et al.* Aging in the CNS: comparison of gray/white matter volume and diffusion tensor data. *Neurobiol Aging* 2008; 29(1): 102-16.
- Al-Izki S, Pryce G, Hankey DJ, Lidster K, von Kutzleben SM, Browne L, *et al.* Lesional-targeting of neuroprotection to the inflammatory penumbra in experimental MS. *Brain : a journal of neurology* 2014; 137(Pt 1): 92-108.
- Allen JS, Bruss J, Brown CK, Damasio H. Normal neuroanatomical variation due to age: the major lobes and a parcellation of the temporal region. *Neurobiol Aging* 2005; 26(9): 1245-60; discussion 79-82.
- Arun T, Tomassini V, Sbardella E, de Ruiter MB, Matthews L, Leite MI, *et al.* Targeting ASIC1 in primary progressive MS: evidence of neuroprotection with amiloride. *Brain : a journal of neurology* 2013; 136(Pt 1): 106-15.
- Bansal N, Szczepaniak L, Ternullo D, Fleckenstein JL, Malloy CR. Effect of exercise on ²³Na MRI and relaxation characteristics of the human calf muscle. *J Magn Reson Imaging* 2000; 11(5): 532-8.
- Barrick TR, Charlton RA, Clark CA, Markus HS. White matter structural decline in normal ageing: a prospective longitudinal study using tract-based spatial statistics. *Neuroimage* 2010; 51(2): 565-77.
- Bartzokis G, Beckson M, Lu PH, Nuechterlein KH, Edwards N, Mintz J. Age-related changes in frontal and temporal lobe volumes in men: a magnetic resonance imaging study. *Arch Gen Psychiatry* 2001; 58(5): 461-5.
- Battaglini M, Jenkinson M, De Stefano N. Evaluating and reducing the impact of white matter lesions on brain volume measurements. *Hum Brain Mapp* 2012; 33(9): 2062-71.
- Bechtold DA, Kapoor R, Smith KJ. Axonal protection using flecainide in experimental autoimmune encephalomyelitis. *Ann Neurol* 2004; 55(5): 607-16.

Bechtold DA, Miller SJ, Dawson AC, Sun Y, Kapoor R, Berry D, *et al.* Axonal protection achieved in a model of MS using lamotrigine. *J Neurol* 2006; 253(12): 1542-51.

Benedetti B, Charil A, Rovaris M, Judica E, Valsasina P, Sormani MP, *et al.* Influence of aging on brain gray and white matter changes assessed by conventional, MT, and DT MRI. *Neurology* 2006; 66(4): 535-9.

Billiet T, Vandenbulcke M, Madler B, Peeters R, Dhollander T, Zhang H, *et al.* Age-related microstructural differences quantified using myelin water imaging and advanced diffusion MRI. *Neurobiol Aging* 2015; 36(6): 2107-21.

Bjartmar C, Trapp BD. Axonal degeneration and progressive neurologic disability in MS. *Neurotox Res* 2003; 5(1-2): 157-64.

Black JA, Dib-Hajj S, Baker D, Newcombe J, Cuzner ML, Waxman SG. Sensory neuron-specific sodium channel SNS is abnormally expressed in the brains of mice with experimental allergic encephalomyelitis and humans with MS. *Proceedings of the National Academy of Sciences of the United States of America* 2000; 97(21): 11598-602.

Black JA, Liu S, Carrithers M, Carrithers LM, Waxman SG. Exacerbation of experimental autoimmune encephalomyelitis after withdrawal of phenytoin and carbamazepine. *Ann Neurol* 2007; 62(1): 21-33.

Black JA, Liu S, Hains BC, Saab CY, Waxman SG. Long-term protection of central axons with phenytoin in monophasic and chronic-relapsing EAE. *Brain* 2006; 129(Pt 12): 3196-208.

Black JA, Newcombe J, Waxman SG. Astrocytes within MS lesions upregulate sodium channel Nav1.5. *Brain* 2010; 133(Pt 3): 835-46.

Blokhin A, Vyshkina T, Komoly S, Kalman B. Variations in mitochondrial DNA copy numbers in MS brains. *Journal of molecular neuroscience : MN* 2008; 35(3): 283-7.

Boada FE GJ, Shen GX, Chang SY, Thulborn KR. Fast three dimensional sodium imaging. *Magn Reson Med* 1997; 37.

Boada FE, Tanase C, Davis D, Walter K, Torres-Trejo A, Couce M, *et al.* Non-invasive assessment of tumor proliferation using triple quantum filtered ²³Na MRI: technical challenges and solutions. *Conf Proc IEEE Eng Med Biol Soc* 2004; 7: 5238-41.

Bodini B, Khaleeli Z, Cercignani M, Miller DH, Thompson AJ, Ciccarelli O. Exploring the relationship between white matter and gray matter damage in early primary progressive MS: an in vivo study with TBSS and VBM. *Hum Brain Mapp* 2009; 30(9): 2852-61.

Boiko T, Rasband MN, Levinson SR, Caldwell JH, Mandel G, Trimmer JS, *et al.* Compact myelin dictates the differential targeting of two sodium channel isoforms in the same axon. *Neuron* 2001; 30(1): 91-104.

Borthakur A, Hancu I, Boada FE, Shen GX, Shapiro EM, Reddy R. In vivo triple quantum filtered twisted projection sodium MRI of human articular cartilage. *J Magn Reson* 1999; 141(2): 286-90.

Cambron M, D'Haeseleer M, Laureys G, Clinckers R, Debruyne J, De Keyser J. White-matter astrocytes, axonal energy metabolism, and axonal degeneration in MS. *Journal of cerebral blood flow and metabolism : official journal of the International Society of Cerebral Blood Flow and Metabolism* 2012; 32(3): 413-24.

Cameron IL, Smith NK, Pool TB, Sparks RL. Intracellular concentration of sodium and other elements as related to mitogenesis and oncogenesis in vivo. *Cancer research* 1980; 40(5): 1493-500.

Campbell GR, Ziabreva I, Reeve AK, Krishnan KJ, Reynolds R, Howell O, *et al.* Mitochondrial DNA deletions and neurodegeneration in MS. *Ann Neurol* 2011; 69(3): 481-92.

Compston A, Coles A. MS. *Lancet* 2008; 372(9648): 1502-17.

Courchesne E, Chisum HJ, Townsend J, Cowles A, Covington J, Egaas B, *et al.* Normal brain development and aging: quantitative analysis at in vivo MR imaging in healthy volunteers. *Radiology* 2000; 216(3): 672-82.

Craner MJ, Damarjian TG, Liu S, Hains BC, Lo AC, Black JA, *et al.* Sodium channels contribute to microglia/macrophage activation and function in EAE and MS. *Glia* 2005; 49(2): 220-9.

Craner MJ, Newcombe J, Black JA, Hartle C, Cuzner ML, Waxman SG. Molecular changes in neurons in MS: altered axonal expression of Nav1.2 and Nav1.6 sodium channels and Na⁺/Ca²⁺ exchanger. *Proc Natl Acad Sci U S A* 2004; 101(21): 8168-73. Epub 2004 May 17.

De Stefano N, Matthews PM, Fu L, Narayanan S, Stanley J, Francis GS, *et al.* Axonal damage correlates with disability in patients with relapsing-remitting MS. Results of a longitudinal magnetic resonance spectroscopy study. *Brain* 1998; 121 (Pt 8): 1469-77.

Dickstein DL, Kabaso D, Rocher AB, Luebke JI, Wearne SL, Hof PR. Changes in the structural complexity of the aged brain. *Aging Cell* 2007; 6(3): 275-84.

Dutta R, McDonough J, Yin X, Peterson J, Chang A, Torres T, *et al.* Mitochondrial dysfunction as a cause of axonal degeneration in MS patients. *Ann Neurol* 2006; 59(3): 478-89.

England JD, Gamboni F, Levinson SR. Increased numbers of sodium channels form along demyelinated axons. *Brain Res* 1991; 548(1-2): 334-7.

Fern R, Ransom BR, Stys PK, Waxman SG. Pharmacological protection of CNS white matter during anoxia: actions of phenytoin, carbamazepine and diazepam. *The Journal of pharmacology and experimental therapeutics* 1993; 266(3): 1549-55.

Fiege DP, Romanzetti S, Mirkes CC, Brenner D, Shah NJ. Simultaneous single-quantum and triple-quantum-filtered MRI of ^{23}Na (SISTINA). *Magn Reson Med* 2013; 69(6): 1691-6.

Filippi M, Preziosa P, Copetti M, Riccitelli G, Horsfield MA, Martinelli V, *et al.* Gray matter damage predicts the accumulation of disability 13 years later in MS. *Neurology* 2013; 81(20): 1759-67.

Fleysher L, Oesingmann N, Brown R, Sodickson DK, Wiggins GC, Inglese M. Noninvasive quantification of intracellular sodium in human brain using ultrahigh-field MRI. *NMR Biomed* 2013a; 26(1): 9-19.

Fleysher L, Oesingmann N, Brown R, Sodickson DK, Wiggins GC, Inglese M. Noninvasive quantification of intracellular sodium in human brain using ultrahigh-field MRI. *NMR Biomed* 2013b; 26(1): 9-19. doi: 0.1002/nbm.2813. Epub 012 Jun 20.

Fleysher L, Oesingmann N, Inglese M. B(0) inhomogeneity-insensitive triple-quantum-filtered sodium imaging using a 12-step phase-cycling scheme. *NMR Biomed* 2010a; 23(10): 1191-8. doi: 10.002/nbm.548.

Fleysher L, Oesingmann N, Inglese M. B(0) inhomogeneity-insensitive triple-quantum-filtered sodium imaging using a 12-step phase-cycling scheme. *NMR Biomed* 2010b; 23(10): 1191-8.

Fotenos AF, Snyder AZ, Girton LE, Morris JC, Buckner RL. Normative estimates of cross-sectional and longitudinal brain volume decline in aging and AD. *Neurology* 2005; 64(6): 1032-9.

Friese MA, Craner MJ, Etzensperger R, Vergo S, Wemmie JA, Welsh MJ, *et al.* Acid-sensing ion channel-1 contributes to axonal degeneration in autoimmune inflammation of the central nervous system. *Nature medicine* 2007; 13(12): 1483-9.

Frischer JM, Bramow S, Dal-Bianco A, Lucchinetti CF, Rauschka H, Schmidbauer M, *et al.* The relation between inflammation and neurodegeneration in MS brains. *Brain* 2009; 132(Pt 5): 1175-89.

Ge Y, Grossman RI, Babb JS, Rabin ML, Mannon LJ, Kolson DL. Age-related total gray matter and white matter changes in normal adult brain. Part I: volumetric MR imaging analysis. *AJNR Am J Neuroradiol* 2002; 23(8): 1327-33.

Giorgio A, Battaglini M, Smith SM, De Stefano N. Brain atrophy assessment in MS: importance and limitations. *Neuroimaging Clin N Am* 2008; 18(4): 675-86, xi.

Giorgio A, Santelli L, Tomassini V, Bosnell R, Smith S, De Stefano N, *et al.* Age-related changes in grey and white matter structure throughout adulthood. *Neuroimage* 2010a; 51(3): 943-51.

Giorgio A, Watkins KE, Chadwick M, James S, Winmill L, Douaud G, *et al.* Longitudinal changes in grey and white matter during adolescence. *Neuroimage* 2010b; 49(1): 94-103.

Good CD, Johnsrude IS, Ashburner J, Henson RN, Friston KJ, Frackowiak RS. A voxel-based morphometric study of ageing in 465 normal adult human brains. *Neuroimage* 2001; 14(1 Pt 1): 21-36.

Guttmann CR, Jolesz FA, Kikinis R, Killiany RJ, Moss MB, Sandor T, *et al.* White matter changes with normal aging. *Neurology* 1998; 50(4): 972-8.

Hancu I, Boada FE, Shen GX. Three-dimensional triple-quantum-filtered (^{23}Na) imaging of in vivo human brain. *Magn Reson Med* 1999; 42(6): 1146-54.

Hedman AM, van Haren NE, Schnack HG, Kahn RS, Hulshoff Pol HE. Human brain changes across the life span: a review of 56 longitudinal magnetic resonance imaging studies. *Hum Brain Mapp* 2012; 33(8): 1987-2002.

Hodgkin AL, Huxley AF. A quantitative description of membrane current and its application to conduction and excitation in nerve. *The Journal of physiology* 1952; 117(4): 500-44.

Hofman PA, Kemerink GJ, Jolles J, Wilmink JT. Quantitative analysis of magnetization transfer images of the brain: effect of closed head injury, age and sex on white matter. *Magn Reson Med* 1999; 42(4): 803-6.

Inglese M, Madelin G, Oesingmann N, Babb JS, Wu W, Stoeckel B, *et al.* Brain tissue sodium concentration in MS: a sodium imaging study at 3 tesla. *Brain* 2010a; 27: 27.

Inglese M, Madelin G, Oesingmann N, Babb JS, Wu W, Stoeckel B, *et al.* Brain tissue sodium concentration in MS: a sodium imaging study at 3 tesla. *Brain : a journal of neurology* 2010b; 133(Pt 3): 847-57.

International MS Genetics C, Beecham AH, Patsopoulos NA, Xifara DK, Davis MF, Kempainen A, *et al.* Analysis of immune-related loci identifies 48 new susceptibility variants for MS. *Nature genetics* 2013; 45(11): 1353-60.

Jain RK. Transport of molecules in the tumor interstitium: a review. *Cancer research* 1987; 47(12): 3039-51.

Jernigan TL, Archibald SL, Fennema-Notestine C, Gamst AC, Stout JC, Bonner J, *et al.* Effects of age on tissues and regions of the cerebrum and cerebellum. *Neurobiol Aging* 2001; 22(4): 581-94.

Kakimoto A, Ito S, Okada H, Nishizawa S, Minoshima S, Ouchi Y. Age-Related Sex-Specific Changes in Brain Metabolism and Morphology. *J Nucl Med* 2016; 57(2): 221-5.

Kapoor R. Neuroprotection in MS: therapeutic strategies and clinical trial design. *Curr Opin Neurol* 2006; 19(3): 255-9.

Kapoor R, Furby J, Hayton T, Smith KJ, Altmann DR, Brenner R, *et al.* Lamotrigine for neuroprotection in secondary progressive MS: a randomised, double-blind, placebo-controlled, parallel-group trial. *The Lancet Neurology* 2010; 9(7): 681-8.

Kemper T, editor. Neuroanatomical and neuropathological changes during aging and dementia. New York: Oxford University Press; 1994.

Koch KS, Leffert HL. Increased sodium ion influx is necessary to initiate rat hepatocyte proliferation. *Cell* 1979; 18(1): 153-63.

Kurtzke JF. Rating neurologic impairment in MS: an expanded disability status scale (EDSS). *Neurology* 1983; 33(11): 1444-52.

Kutzelnigg A, Lucchinetti CF, Stadelmann C, Bruck W, Rauschka H, Bergmann M, *et al.* Cortical demyelination and diffuse white matter injury in MS. *Brain* 2005; 128(Pt 11): 2705-12.

Lang F. Mechanisms and significance of cell volume regulation. *Journal of the American College of Nutrition* 2007; 26(5 Suppl): 613S-23S.

Lassmann H. MS: is there neurodegeneration independent from inflammation? *Journal of the neurological sciences* 2007; 259(1-2): 3-6.

Lassmann H. Mechanisms of white matter damage in MS. *Glia* 2014; 62(11): 1816-30.

Lassmann H, van Horssen J, Mahad D. Progressive MS: pathology and pathogenesis. *Nature reviews Neurology* 2012; 8(11): 647-56.

Liu RS, Lemieux L, Bell GS, Sisodiya SM, Shorvon SD, Sander JW, *et al.* A longitudinal study of brain morphometrics using quantitative magnetic resonance imaging and difference image analysis. *Neuroimage* 2003; 20(1): 22-33.

Lo AC, Saab CY, Black JA, Waxman SG. Phenytoin protects spinal cord axons and preserves axonal conduction and neurological function in a model of neuroinflammation in vivo. *Journal of neurophysiology* 2003; 90(5): 3566-71.

Lublin FD, Reingold SC. Defining the clinical course of MS: results of an international survey. *National MS Society (USA) Advisory Committee on Clinical Trials of New Agents in MS. Neurology* 1996; 46(4): 907-11.

Maarouf A, Audoin B, Konstantin S, Rico A, Soulier E, Reuter F, *et al.* Topography of brain sodium accumulation in progressive MS. *Magma* 2014; 27(1): 53-62.

Madelin G, Kline R, Walvick R, Regatte RR. A method for estimating intracellular sodium concentration and extracellular volume fraction in brain in vivo using sodium magnetic resonance imaging. *Sci Rep* 2014; 4: 4763.

Magliozzi R, Howell OW, Reeves C, Roncaroli F, Nicholas R, Serafini B, *et al.* A Gradient of neuronal loss and meningeal inflammation in MS. *Ann Neurol* 2010; 68(4): 477-93.

Marnier L, Nyengaard JR, Tang Y, Pakkenberg B. Marked loss of myelinated nerve fibers in the human brain with age. *J Comp Neurol* 2003; 462(2): 144-52.

Matthies C, Nagel AM, Schad LR, Bachert P. Reduction of B(0) inhomogeneity effects in triple-quantum-filtered sodium imaging. *J Magn Reson* 2010; 202(2): 239-44.

Maudsley AA, Hilal SK. Biological aspects of sodium-23 imaging. *Br Med Bull* 1984; 40(2): 165-6.

McDonald WI, Compston A, Edan G, Goodkin D, Hartung HP, Lublin FD, *et al.* Recommended diagnostic criteria for MS: guidelines from the International Panel on the diagnosis of MS. *Ann Neurol* 2001; 50(1): 121-7.

McLaughlin NC, Paul RH, Grieve SM, Williams LM, Laidlaw D, DiCarlo M, *et al.* Diffusion tensor imaging of the corpus callosum: a cross-sectional study across the lifespan. *Int J Dev Neurosci* 2007; 25(4): 215-21.

Meier-Ruge W, Ulrich J, Bruhlmann M, Meier E. Age-related white matter atrophy in the human brain. *Ann N Y Acad Sci* 1992; 673: 260-9.

Mellon EA, Pilkinton DT, Clark CM, Elliott MA, Witschey WR, 2nd, Borthakur A, *et al.* Sodium MR imaging detection of mild Alzheimer disease: preliminary study. *AJNR American journal of neuroradiology* 2009; 30(5): 978-84.

Miller DH, Barkhof F, Frank JA, Parker GJ, Thompson AJ. Measurement of atrophy in MS: pathological basis, methodological aspects and clinical relevance. *Brain* 2002; 125(Pt 8): 1676-95.

Moll C, Mourre C, Lazdunski M, Ulrich J. Increase of sodium channels in demyelinated lesions of MS. *Brain Res* 1991; 556(2): 311-6.

Muller N, Bodenhausen G, RR E. Relaxation-Induced Violations of Coherence Transfer Selection Rules in Nuclear Magnetic Resonance. *J Magn Reson* 1987; 75: 297-334.

Nagy I, Lustyik G, Lukacs G, Nagy V, Balazs G. Correlation of malignancy with the intracellular Na⁺:K⁺ ratio in human thyroid tumors. *Cancer research* 1983; 43(11): 5395-402.

Nave KA, Trapp BD. Axon-glia signaling and the glial support of axon function. *Annual review of neuroscience* 2008; 31: 535-61.

Nikic I, Merkler D, Sorbara C, Brinkoetter M, Kreutzfeldt M, Bareyre FM, *et al.* A reversible form of axon damage in experimental autoimmune encephalomyelitis and MS. *Nat Med* 2011; 17(4): 495-9.

Nikolaeva MA, Mukherjee B, Stys PK. Na⁺-dependent sources of intra-axonal Ca²⁺ release in rat optic nerve during in vitro chemical ischemia. *The Journal of neuroscience : the official journal of the Society for Neuroscience* 2005; 25(43): 9960-7.

Noseworthy JH, Lucchinetti C, Rodriguez M, Weinshenker BG. MS. *N Engl J Med* 2000; 343(13): 938-52.

O'Dwyer L, Lamberton F, Bokde AL, Ewers M, Faluyi YO, Tanner C, *et al.* Sexual dimorphism in healthy aging and mild cognitive impairment: a DTI study. *PLoS One* 2012; 7(7): e37021.

O'Malley HA, Shreiner AB, Chen GH, Huffnagle GB, Isom LL. Loss of Na⁺ channel beta2 subunits is neuroprotective in a mouse model of MS. *Molecular and cellular neurosciences* 2009; 40(2): 143-55.

Ota M, Obata T, Akine Y, Ito H, Ikehira H, Asada T, *et al.* Age-related degeneration of corpus callosum measured with diffusion tensor imaging. *Neuroimage* 2006; 31(4): 1445-52.

Ouardouz M, Malek S, Coderre E, Stys PK. Complex interplay between glutamate receptors and intracellular Ca²⁺ stores during ischaemia in rat spinal cord white matter. *J Physiol* 2006; 577(Pt 1): 191-204.

Ouwerkerk R, Bleich KB, Gillen JS, Pomper MG, Bottomley PA. Tissue sodium concentration in human brain tumors as measured with ²³Na MR imaging. *Radiology* 2003; 227(2): 529-37. Epub 2003 Mar 27.

Pagani E, Agosta F, Rocca MA, Caputo D, Filippi M. Voxel-based analysis derived from fractional anisotropy images of white matter volume changes with aging. *Neuroimage* 2008; 41(3): 657-67.

Paling D, Solanky BS, Riemer F, Tozer DJ, Wheeler-Kingshott CA, Kapoor R, *et al.* Sodium accumulation is associated with disability and a progressive course in MS. *Brain* 2013; 136(Pt 7): 2305-17.

Perier O, Gregoire A. Electron microscopic features of MS lesions. *Brain* 1965; 88(5): 937-52.

Petracca M, Vancea RO, Fleysher L, Jonkman LE, Oesingmann N, Inglese M. Brain intra- and extracellular sodium concentration in MS: a 7 T MRI study. *Brain* 2016.

Pfefferbaum A, Adalsteinsson E, Sullivan EV. Frontal circuitry degradation marks healthy adult aging: Evidence from diffusion tensor imaging. *Neuroimage* 2005; 26(3): 891-9.

Pitt D, Werner P, Raine CS. Glutamate excitotoxicity in a model of MS. *Nature medicine* 2000; 6(1): 67-70.

Politis M, Giannetti P, Su P, Turkheimer F, Keihaninejad S, Wu K, *et al.* Increased PK11195 PET binding in the cortex of patients with MS correlates with disability. *Neurology* 2012; 79(6): 523-30.

Polman CH, Reingold SC, Banwell B, Clanet M, Cohen JA, Filippi M, *et al.* Diagnostic criteria for MS: 2010 revisions to the McDonald criteria. *Annals of neurology* 2011; 69(2): 292-302.

Randall AD, Booth C, Brown JT. Age-related changes to Na⁺ channel gating contribute to modified intrinsic neuronal excitability. *Neurobiol Aging* 2012; 33(11): 2715-20.

Raz N, Rodrigue KM. Differential aging of the brain: patterns, cognitive correlates and modifiers. *Neurosci Biobehav Rev* 2006; 30(6): 730-48.

Rees S, editor. *A quantitative electron microscopic study of aging human cerebral cortex*. Berlin; 1976.

Rizzo V, Richman J, Puthanveetil SV. Dissecting mechanisms of brain aging by studying the intrinsic excitability of neurons. *Front Aging Neurosci* 2014; 6: 337.

Rossi F, Giorgio A, Battaglini M, Stromillo ML, Portaccio E, Goretti B, *et al.* Relevance of brain lesion location to cognition in relapsing MS. *PLoS One* 2012; 7(11): e44826.

Rovaris M, Iannucci G, Cercignani M, Sormani MP, De Stefano N, Gerevini S, *et al.* Age-related changes in conventional, magnetization transfer, and diffusion-tensor MR imaging findings: study with whole-brain tissue histogram analysis. *Radiology* 2003; 227(3): 731-8.

Rush AM, Dib-Hajj SD, Waxman SG. Electrophysiological properties of two axonal sodium channels, Nav1.2 and Nav1.6, expressed in mouse spinal sensory neurones. *J Physiol* 2005; 564(Pt 3): 803-15. Epub 2005 Mar 10.

Sailer M, Fischl B, Salat D, Tempelmann C, Schonfeld MA, Busa E, *et al.* Focal thinning of the cerebral cortex in MS. *Brain* 2003; 126(Pt 8): 1734-44.

Sala S, Agosta F, Pagani E, Copetti M, Comi G, Filippi M. Microstructural changes and atrophy in brain white matter tracts with aging. *Neurobiol Aging* 2012; 33(3): 488-98 e2.

Salat DH, Kaye JA, Janowsky JS. Prefrontal gray and white matter volumes in healthy aging and Alzheimer disease. *Arch Neurol* 1999; 56(3): 338-44.

Salat DH, Tuch DS, Greve DN, van der Kouwe AJ, Hevelone ND, Zaleta AK, *et al.* Age-related alterations in white matter microstructure measured by diffusion tensor imaging. *Neurobiol Aging* 2005; 26(8): 1215-27.

Smith KJ. Sodium channels and MS: roles in symptom production, damage and therapy. *Brain Pathol* 2007; 17(2): 230-42.

Smith SM. Fast robust automated brain extraction. *Hum Brain Mapp* 2002; 17(3): 143-55.

Sowell ER, Thompson PM, Toga AW. Mapping changes in the human cortex throughout the span of life. *Neuroscientist* 2004; 10(4): 372-92.

Stobbe R, Beaulieu C. In vivo sodium magnetic resonance imaging of the human brain using soft inversion recovery fluid attenuation. *Magn Reson Med* 2005; 54(5): 1305-10.

Stys PK. Protective effects of antiarrhythmic agents against anoxic injury in CNS white matter. *Journal of cerebral blood flow and metabolism : official journal of the International Society of Cerebral Blood Flow and Metabolism* 1995; 15(3): 425-32.

Stys PK. General mechanisms of axonal damage and its prevention. *J Neurol Sci* 2005; 233(1-2): 3-13.

Stys PK, Lesiuk H. Correlation between electrophysiological effects of mexiletine and ischemic protection in central nervous system white matter. *Neuroscience* 1996; 71(1): 27-36.

Stys PK, Ransom BR, Waxman SG. Tertiary and quaternary local anesthetics protect CNS white matter from anoxic injury at concentrations that do not block excitability. *Journal of neurophysiology* 1992a; 67(1): 236-40.

Stys PK, Sontheimer H, Ransom BR, Waxman SG. Noninactivating, tetrodotoxin-sensitive Na⁺ conductance in rat optic nerve axons. *Proc Natl Acad Sci U S A* 1993; 90(15): 6976-80.

Stys PK, Waxman SG, Ransom BR. Ionic mechanisms of anoxic injury in mammalian CNS white matter: role of Na⁺ channels and Na⁽⁺⁾-Ca²⁺ exchanger. *The Journal of neuroscience : the official journal of the Society for Neuroscience* 1992b; 12(2): 430-9.

Sullivan EV, Adalsteinsson E, Pfefferbaum A. Selective age-related degradation of anterior callosal fiber bundles quantified in vivo with fiber tracking. *Cereb Cortex* 2006; 16(7): 1030-9.

Tallantyre EC, Bo L, Al-Rawashdeh O, Owens T, Polman CH, Lowe JS, *et al.* Clinico-pathological evidence that axonal loss underlies disability in progressive MS. *Mult Scler* 2010; 16(4): 406-11.

Tanase C, Boada FE. Triple-quantum-filtered imaging of sodium in presence of B(0) inhomogeneities. *J Magn Reson* 2005; 174(2): 270-8.

Tang Y, Nyengaard JR, Pakkenberg B, Gundersen HJ. Age-induced white matter changes in the human brain: a stereological investigation. *Neurobiol Aging* 1997; 18(6): 609-15.

Taylor CP. Na⁺ currents that fail to inactivate. *Trends Neurosci* 1993; 16(11): 455-60.

Thulborn KR, Davis D, Adams H, Gindin T, Zhou J. Quantitative tissue sodium concentration mapping of the growth of focal cerebral tumors with sodium magnetic resonance imaging. *Magnetic resonance in medicine : official journal of the Society of Magnetic Resonance in Medicine / Society of Magnetic Resonance in Medicine* 1999a; 41(2): 351-9.

Thulborn KR, Davis D, Snyder J, Yonas H, Kassam A. Sodium MR imaging of acute and subacute stroke for assessment of tissue viability. *Neuroimaging Clin N Am* 2005; 15(3): 639-53, xi-xii.

Thulborn KR, Gindin TS, Davis D, Erb P. Comprehensive MR imaging protocol for stroke management: tissue sodium concentration as a measure of tissue viability in nonhuman primate studies and in clinical studies. *Radiology* 1999b; 213(1): 156-66.

Trapp BD, Peterson J, Ransohoff RM, Rudick R, Mork S, Bo L. Axonal transection in the lesions of MS. *N Engl J Med* 1998; 338(5): 278-85.

Trapp BD, Stys PK. Virtual hypoxia and chronic necrosis of demyelinated axons in MS. *The Lancet Neurology* 2009; 8(3): 280-91.

Tsang A, Stobbe RW, Beaulieu C. Triple-quantum-filtered sodium imaging of the human brain at 4.7 T. *Magn Reson Med* 2012; 67(6): 1633-43.

Tsang A, Stobbe RW, Beaulieu C. In vivo double quantum filtered sodium magnetic resonance imaging of human brain. *Magn Reson Med* 2015; 73(2): 497-504.

Turski PA, Perman WH, Hald JK, Houston LW, Strother CM, Sackett JF. Clinical and experimental vasogenic edema: in vivo sodium MR imaging. Work in progress. *Radiology* 1986; 160(3): 821-5.

Vergo S, Craner MJ, Etzensperger R, Attfield K, Friese MA, Newcombe J, *et al.* Acid-sensing ion channel 1 is involved in both axonal injury and demyelination in MS and its animal model. *Brain : a journal of neurology* 2011; 134(Pt 2): 571-84.

Walhovd KB, Fjell AM, Reinvang I, Lundervold A, Dale AM, Eilertsen DE, *et al.* Effects of age on volumes of cortex, white matter and subcortical structures. *Neurobiol Aging* 2005; 26(9): 1261-70; discussion 75-8.

Waxman SG. Conduction in Myelinated, Unmyelinated,

and Demyelinated Fibers. *Arch Neurol* 1977; 34.

Waxman SG. Axonal conduction and injury in MS: the role of sodium channels. *Nat Rev Neurosci* 2006a; 7(12): 932-41.

Waxman SG. Ions, energy and axonal injury: towards a molecular neurology of MS. *Trends in molecular medicine* 2006b; 12(5): 192-5.

Waxman SG. Mechanisms of disease: sodium channels and neuroprotection in MS-current status. *Nature clinical practice Neurology* 2008; 4(3): 159-69.

West RL. An application of prefrontal cortex function theory to cognitive aging. *Psychol Bull* 1996; 120(2): 272-92.

Wiggins GC, Brown R., Fleysher L., Zhang B., Stoeckel B., Inglese M., *et al.* A Nested Dual Frequency Birdcage/Stripline Coil for Sodium/Proton Brain Imaging at 7T. *Proceedings of ISMRM 2010* 2010: 1500.

Winter PM, Bansal N. Triple-quantum-filtered (^{23}Na) NMR spectroscopy of subcutaneously implanted 9L gliosarcoma in the rat in the presence of TmDOTP(5-1). *J Magn Reson* 2001; 152(1): 70-8.

Winter PM, Seshan V, Makos JD, Sherry AD, Malloy CR, Bansal N. Quantitation of intracellular $[\text{Na}^+]$ in vivo by using TmDOTP5- as an NMR shift reagent and extracellular marker. *Journal of applied physiology* 1998; 85(5): 1806-12.

Woodward DL, Reed DJ, Woodbury DM. Extracellular space of rat cerebral cortex. *The American journal of physiology* 1967; 212(2): 367-70.

Zaaraoui W, Konstandin S, Audoin B, Nagel AM, Rico A, Malikova I, *et al.* Distribution of brain sodium accumulation correlates with disability in MS: a cross-sectional ^{23}Na MR imaging study. *Radiology* 2012; 264(3): 859-67.